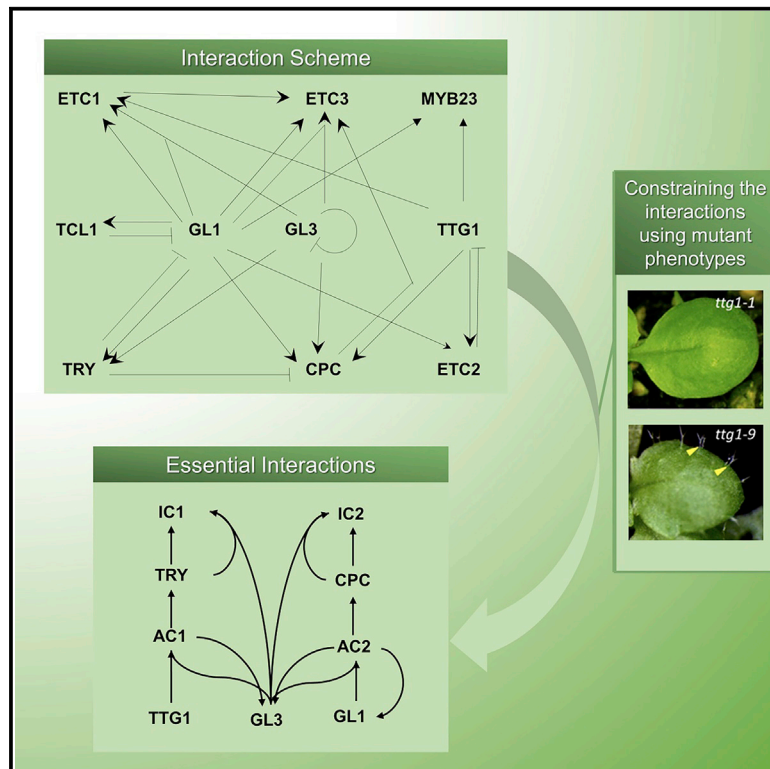


# Identification of the Trichome Patterning Core Network Using Data from Weak *ttg1* Alleles to Constrain the Model Space

## Graphical Abstract



## Authors

Rachappa Balkunde, Anna Deneer, Hanna Bechtel, ..., Benjamin Jaegle, Christian Fleck, Martin Hülskamp

## Correspondence

christian.fleck@bsse.ethz.ch (C.F.), martin.huelskamp@uni-koeln.de (M.H.)

## In Brief

Mathematical modeling of developmental processes is challenging because most of the parameters are normally unknown. Balkunde et al. use weak trichome patterning mutants to constrain the data and use global mathematical methods to identify the core parts of the complex gene regulatory network that are essential for patterning.

## Highlights

- Complex changes in trichome patterning are explained by reduced TTTG1 GL3 interaction
- Mathematical modeling and data constraint reveal the network structure
- Trichome patterning requires an activator-inhibitor and an activator-diffusion mechanism
- Trichome patterning requires two pathways activating long- and short-range inhibitors



## Article

# Identification of the Trichome Patterning Core Network Using Data from Weak *ttg1* Alleles to Constrain the Model Space

Rachappa Balkunde,<sup>1,3,6</sup> Anna Deneer,<sup>2,6</sup> Hanna Bechtel,<sup>1</sup> Bipei Zhang,<sup>1</sup> Stefanie Herberth,<sup>1</sup> Martina Pesch,<sup>1</sup> Benjamin Jaegle,<sup>1,4</sup> Christian Fleck,<sup>2,5,\*</sup> and Martin Hülskamp<sup>1,7,\*</sup>

<sup>1</sup>Botanical Institute, Biocenter, Cologne University, 50674 Cologne, Germany

<sup>2</sup>Lab for Systems and Synthetic Biology and Biometrics, Department of Mathematical and Statistical Methods, Wageningen University, 6700 HB, Wageningen, The Netherlands

<sup>3</sup>Present address: Biology Department, Washington University in St. Louis, St. Louis, MO 63130, USA

<sup>4</sup>Present address: Gregor Mendel Institute of Molecular Plant Biology, 1030 Vienna, Austria

<sup>5</sup>Present address: Department of Biosystems Science and Engineering, ETH Zurich, 4058 Basel, Switzerland

<sup>6</sup>These authors contributed equally

<sup>7</sup>Lead Contact

\*Correspondence: [christian.fleck@bsse.ethz.ch](mailto:christian.fleck@bsse.ethz.ch) (C.F.), [martin.huelskamp@uni-koeln.de](mailto:martin.huelskamp@uni-koeln.de) (M.H.)  
<https://doi.org/10.1016/j.celrep.2020.108497>

## SUMMARY

The regular distribution of trichomes on leaves in *Arabidopsis* is a well-understood model system for two-dimensional pattern formation. It involves more than 10 genes and is governed by two patterning principles, the activator-inhibitor (AI) and the activator-depletion (AD) mechanisms, though their relative contributions are unknown. The complexity of gene interactions, protein interactions, and intra- and intercellular mobility of proteins makes it very challenging to understand which aspects are relevant for pattern formation. In this study, we use global mathematical methods combined with a constraining of data to identify the structure of the underlying network. To constrain the model, we perform a genetic, cell biological, and biochemical study of weak *ttg1* alleles. We find that the core of trichome patterning is a combination of AI and AD mechanisms differentiating between two pathways activating the long-range inhibitor CPC and the short-range inhibitor TRY.

## INTRODUCTION

Mathematical modeling has become an integrated discipline in developmental biology aiming to integrate the knowledge about a biological system in order to arrive at either conceptual statements or predictions about the consequences of experimental manipulations. One frequent problem, however, is that the available datasets do not contain enough information for the parameters of the mathematical model to be uniquely identified. This means that the model is capable of reproducing the data with many different parameters, and this may lead to the undesirable situation that no clear conceptual statements can be made and many different model predictions are possible. The way out of this situation is to use global analysis methods in combination with further constraining observations or data. It is possible, although challenging, to use mathematical modeling approaches in these situations and arrive at conceptual statements on the developmental process despite the incomplete information about the biological system. Trichome patterning in *Arabidopsis* is an excellent model system for which this constraint global analysis method needs to be applied. On the one hand, it presents a fairly simple developmental process that can be described as a two-dimensional pattern formation (Pesch and

Hülskamp, 2004). On the other hand, the underlying gene regulatory network involves many gene interactions, protein-protein interactions, and intercellular transport processes for which the parameters are largely unknown (Pesch and Hülskamp, 2009).

Our understanding of trichome formation in *Arabidopsis thaliana* is based on the genetic identification of the key genes and a detailed molecular and cell biological analysis (Balkunde et al., 2010; Grebe, 2012; Pesch and Hülskamp, 2009; Tominaga-Wada et al., 2011). Trichomes are initiated without reference to already existing positional information with a regular spacing. Although there is a remarkable degree of variability in the relative distances (Greese et al., 2012), trichomes are normally not found immediately next to each other (Hülskamp et al., 1994). This pattern is established early during leaf development. On young rosette leaves incipient trichomes are typically separated by three or four epidermal cells, and their distance is increased during leaf expansion because of cell divisions and growth of the intervening cells (Hülskamp et al., 1994). Trichome patterning in *Arabidopsis thaliana* is regulated by a gene regulatory network involving trichome-promoting and trichome-inhibiting genes. Three genes act as the major positive regulators: *TRANSPARENT TESTA GLABRA1* (*TTG1*) encodes a WD40 protein (Galway et al., 1994; Koornneef, 1981; Walker



et al., 1999), *GLABRA1* (*GL1*) encodes a R2R3-MYB-related transcription factor (Oppenheimer et al., 1991), and *GLABRA3* (*GL3*) encodes a basic helix-loop-helix (bHLH)-like transcription factor (Hülkamp et al., 1994; Koornneef et al., 1982; Payne et al., 2000). In addition, *MYB23* and *EGL3* act in a partially redundant manner with *GL1* and *GL3*, respectively (Kirik et al., 2001, 2005b; Zhang et al., 2003a). *TRIPTYCHON* (*TRY*) and *CAPRICE* (*CPC*) represent negative regulators of trichome development, as the corresponding single mutants show trichome clusters and a higher trichome density, respectively (Hülkamp et al., 1994; Schellmann et al., 2002; Wada et al., 1997). They encode R3 single-repeat MYB proteins and act partially redundant with five additional homologs (Gan et al., 2011; Kirik et al., 2004a, 2004b; Schellmann et al., 2002; Tomi-naga et al., 2008; Wang et al., 2007, 2008, 2010; Wester et al., 2009).

The trichome-promoting and inhibiting proteins show a complex protein interaction pattern. TTG1 and GL1 both bind to GL3/EGL3 (Digiuni et al., 2008; Gao et al., 2008; Kirik et al., 2005a; Payne et al., 2000; Wang and Chen, 2008; Zhang et al., 2003a; Zhao et al., 2008; Zimmermann et al., 2004), and the binding of one of them counteracts the binding of the other to GL3 (Pesch et al., 2015). This competitive behavior is also seen at the level of target gene regulation such that the transcriptional activation of TRY by GL3 and TTG1 is counteracted by GL1 and the activation of CPC by GL3 and GL1 is inhibited by TTG1 (Pesch et al., 2015). Also, the negative regulators bind to GL3/EGL3, thereby preventing the binding of GL1 (Bernhardt et al., 2003; Esch et al., 2003; Payne et al., 2000).

Theoretical models have been developed to explain how the gene regulatory network formed by the activators and inhibitors can create a *de novo* trichome pattern (Benítez et al., 2008; Benítez et al., 2007; Bouyer et al., 2008; Digiuni et al., 2008). The molecular interaction schemes are consistent with two general principles, an activator-inhibitor (AI) model and an activator-depletion (AD) model (Pesch and Hülkamp, 2009). According to the AI model, the activators promote the expression of the inhibitors. The inhibitors move between cells and repress the activators in the neighborhood. The AD model explains the establishment of a trichome-pattern patterning by the depletion of the activator in the neighborhood of trichome initials. It is based on the finding that TTG1 can move between cells and that TTG1 is trapped in trichome initials by binding to GL3 (Balkunde et al., 2011; Bouyer et al., 2008). Both principles are able to generate regular spacing patterns *de novo* (Meinhardt and Gierer, 1974). While the experimental data support the existence of both mechanisms, it is very difficult to assess their individual biological significance, because the two mechanisms involve the same genes.

Both the AI and AD models had been primarily used to demonstrate the minimal requirements to describe trichome patterning. Most importantly, the models do not “need” the additional genes that are, however, known to act in the network. In this study, we constrain the model to unfold structural elements by analyzing the TTG1 gene in greater detail. TTG1 appears to be a key component in the AI model as well as the AD model. We focus on the molecular function of weak *ttg1* alleles. While strong *ttg1* alleles are devoid of trichomes, weak *ttg1* alleles produce a reduced number of trichomes (Koornneef, 1981; Larkin et al.,

1994, 1999; Long and Schiefelbein, 2020; Walker et al., 1999). Remarkably, all weak *ttg1* alleles exhibit trichome clusters. It was possible to predict this unusual behavior of TTG1 alleles by changing several parameters of the TTG1 function in the AD model (Bouyer et al., 2008). It is not known whether the role of TTG1 in the AI model also contributes to the phenotype of weak *ttg1* alleles and, if so, what the relative contributions of the AD and AI mechanisms are. According to the AD model, cluster formation can be explained by a failure to remove TTG1 from the neighborhood of trichome initials. In the AI model, cluster formation in weak *ttg1* alleles could be explained if TRY would not be expressed. We show that the interaction of mutant TTG1 proteins carrying the point mutations of the weak *ttg1* alleles with GL3 protein are strongly impaired and that mutant TTG1 protein is not depleted around trichomes. We further show that TRY expression, but not CPC expression, is strongly reduced in *ttg1* alleles. We developed a mathematical model that combines the AI and AD models. We reveal the requirement of additional structural elements in the network and demonstrate that the reduced interaction of TTG1 to GL3 is sufficient to explain all trichome phenotypes of weak *ttg1* mutants.

## RESULTS

### Weak *ttg1* Alleles Exhibit Irregular Spatial Distribution of Trichomes

Strong *ttg1* alleles show a glabrous phenotype indicating that TTG1 has a positive role in trichome formation. All weak alleles exhibit a cluster phenotype (Koornneef, 1981; Larkin et al., 1999; Walker et al., 1999), suggesting a negative function in trichome formation (Figure 1A). Thus, strong and weak *ttg1* alleles appear to have opposite genetic functions. Interestingly, this is specific to the trichome trait, as seed color, seed coat mucilage, and root hair formation phenotypes do not show the opposite phenotype in the weak *ttg1* alleles *ttg1-9*, *ttg1-11*, and *ttg1-12* (Figure S1). To understand the molecular basis of cluster formation in the weak *ttg1* alleles, we analyzed the three weak *ttg1* alleles *ttg1-9* (Larkin et al., 1994; Walker et al., 1999), *ttg1-11*, and *ttg1-12* (Larkin et al., 1994, 1999) in more detail using two strong *ttg1* alleles, *ttg1-1* (Koornneef, 1981) and *ttg1-13* (Larkin et al., 1999), as a reference. The three weak alleles have point mutations leading to amino acid exchanges at different positions (Koornneef, 1981; Larkin et al., 1994, 1999; Walker et al., 1999) (Table S1).

During the phenotypic analysis of the three weak *ttg1* alleles, we noticed that trichomes appeared to be less regularly distributed compared to wild type, suggesting a randomized trichome pattern. We used TrichEratops to generate coordinates (Failmezger et al., 2013). We limit the analysis to the *ttg1-9* allele, because *ttg1-11* and *ttg1-12* alleles produce too few trichomes on each leaf to yield sufficient data for a meaningful statistical analysis. To quantitatively compare the regularity of trichome patterns on wild-type and *ttg1-9* leaves, we used different measures.

As a first measure we use the coefficient of variation (CV) of the nearest neighbor distances distribution ( $CV_{NN}$ ), which is defined as the standard deviation normalized by the mean of the nearest neighbor distances (Figure 1B). For wild type, we found a regular, but not perfect, pattern (Greese et al., 2012) with a CV of  $0.33 \pm 0.05$ . The *ttg1-9* allele exhibits a more irregular pattern,

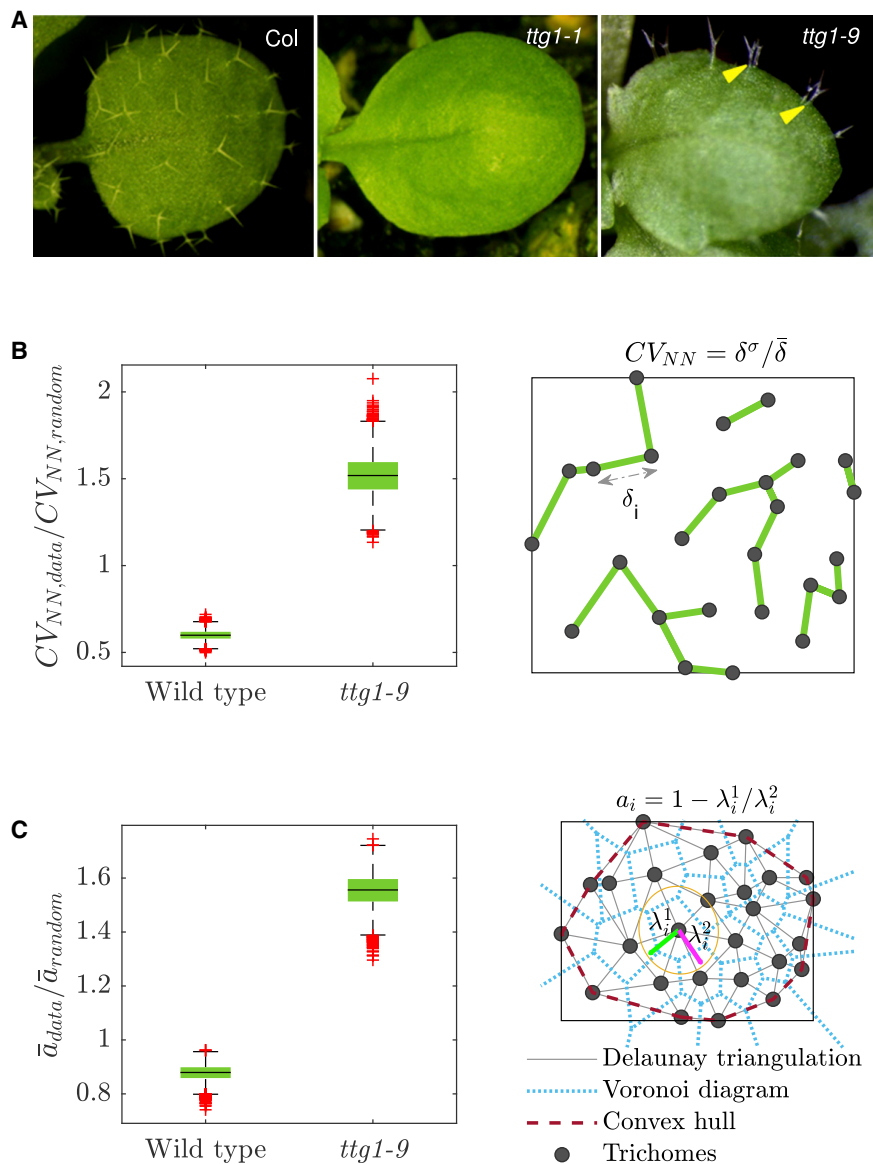


**Figure 1. Trichome Patterning Defects in *ttg1-9* Leaves**

(A) Fourth rosette leaves of wild type and *ttg1-1* and *ttg1-9* mutants. Note, that the strong *ttg1-1* allele has no trichomes, while the weak *ttg1-9* allele exhibits clusters (yellow arrowheads). Scale bars, 1 cm.

(B and C) Comparison of measures of randomness between wild-type or *ttg1-9* data and corresponding random references. The left column shows the distribution of the different measures for bootstrapped data from leaves relative to simulations of random patterns. The right column shows an example wild-type leaf where the different measures are visualized, corresponding to the boxplots on the left side. (B) Nearest neighbor distances.  $\delta^\sigma$  represents the standard deviations and  $\bar{\delta}$  the mean of the nearest neighbor distances. (C) Mean anisotropy, defined as the ratio of the eigenvalues as a measure of deviation from isotropy. A smaller anisotropy indicates a more regular pattern.

with a mean CV of  $0.84 \pm 0.22$ . Next, we compared the leaf phenotypes to randomly generated point patterns. For the random patterns, we consider the difference between the trichome densities for wild type and *ttg1-9* and simulate 10,000 instances, where for each instance, the points are placed with a uniform probability across the simulated region. Using the bootstrapping method, we generate 10,000 samples based on the  $CV_{NN}$  distribution from the leaves and compare the bootstrap distributions with the random references (Figure 1B). In this comparison, we

show that the wild-type pattern exhibits significantly less variability in trichome distances than the corresponding random reference (one-tailed Mann-Whitney *U* test,  $p < 0.01$ ), whereas the *ttg1-9* allele shows a higher irregularity than the random distribution with similar density ( $p < 0.01$ ).

Because the nearest neighbor distances give a very narrow viewpoint on the region around a trichome, we decided to employ another quantifications of the variability, which takes into account a more appropriate region of interest. Toward this

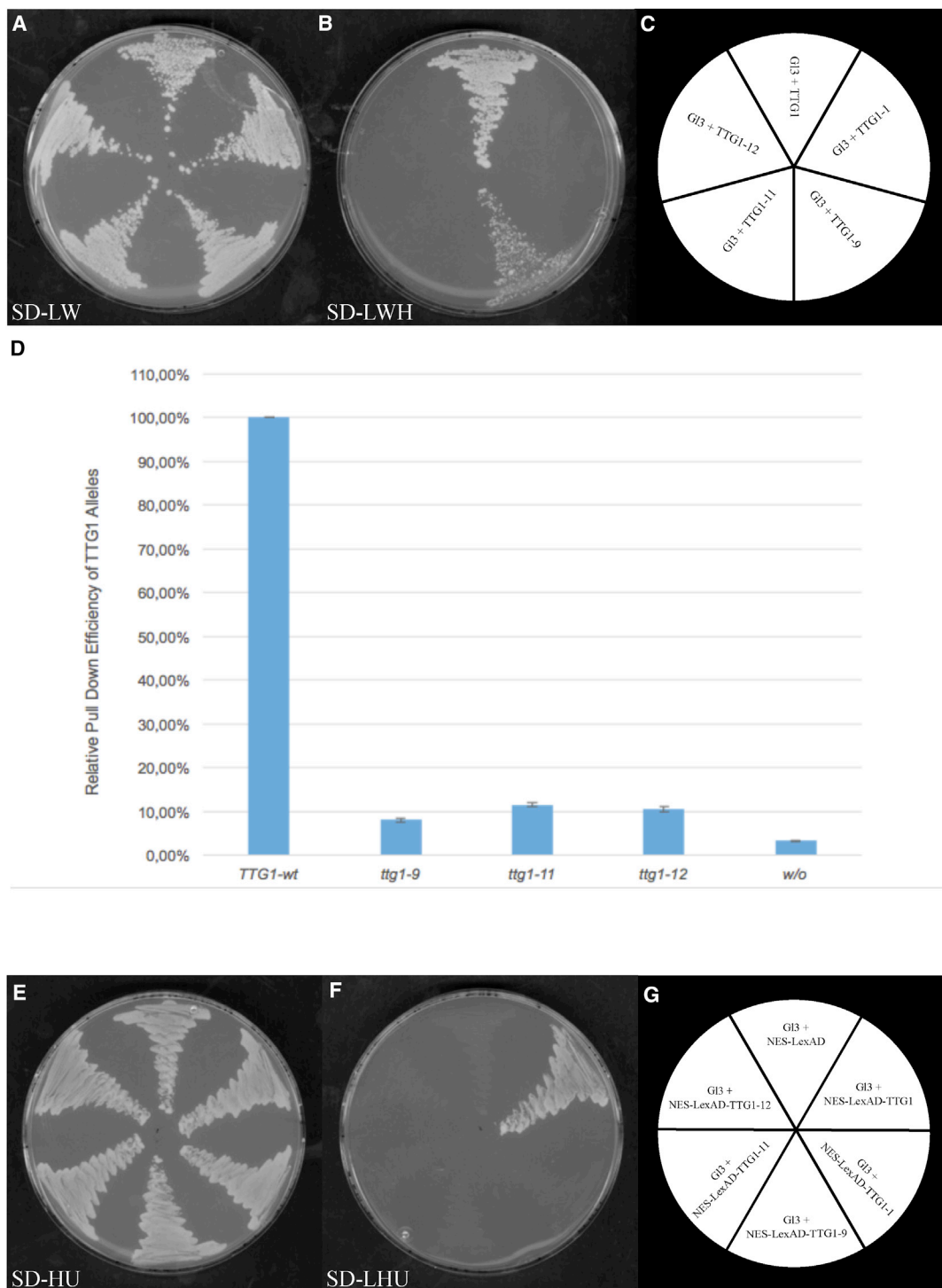


**Figure 2. Protein-Protein Interactions and Nuclear Transport of Wild-Type and Mutant TTG1 Proteins**

(A–C) Protein-protein interactions between TTG1 mutant proteins and GL3. (A) Control for presence of plasmids. (B) Interaction assay on medium supplemented with 5 mM 3-aminotriazole (3-AT). Yeast growth indicates positive interactions. (C) Schematic presentation showing the positions of different combination on the plates.

(legend continued on next page)

end, we calculated the anisotropy of the neighborhood around the trichomes (Greese et al., 2012) (Figure 1C). The anisotropy from the experimental data is taken relative to the corresponding random references. Comparing between the anisotropy of bootstrapped experimental results and the random references, we come to the same conclusion as for the  $CV_{NN}$ . Testing between wild type and *ttg1-9* showed that the *ttg1-9* allele has a significantly higher relative mean anisotropy (one-tailed Mann-Whitney *U* test,  $p < 0.01$ ), confirming that *ttg1-9* distributions are more irregular than wild type.

For a hypothetical homogeneous (not depending on space) random trichome pattern, the cluster probability depends inversely on the trichome density (Figure S2A). Thus, *ttg1-9* mutants should have fewer clusters than wild type. This is calculated for wild type and *ttg1-9* in Figure S2A. Thus, cluster formation in *ttg1-9* mutants cannot be explained in full by a homogeneous random process, suggesting that it is due to a deterministic process. To differentiate between stochastic processes and deterministic processes that only appear random, we determined the correlation dimension (Theiler, 1987). It gives an estimate of the number of parameters needed to explain the measured variability. We find for both wild-type and *ttg1-9* data a correlation dimension smaller than the homogeneous random patterning process (Figures S2C–S2F), indicating that deterministic factors control a considerable part of the variability in trichome distances. The theoretically expected probability of clusters is not dependent on the area available for trichome formation (Figure S2B), suggesting that these deterministic factors are represented by altered genetic interactions in *ttg1-9* mutants.

### Amino Acid Exchanges in Weak TTG1 Alleles Reduce/Abolish the Interaction with GL3, EGL3, and TT8

To explore the molecular function of the weak *ttg1* alleles, we studied the protein interaction of TTG1 with GL3. TTG1 is considered to regulate trichome formation by binding to GL3. It has been shown before that the TTG1 protein lacking the 26 C-terminal amino acids (corresponding to the *ttg1-1* allele) does not interact with GL3 (Balkunde et al., 2011; Payne et al., 2000) and that two recently identified weak alleles, *ttg1-23* and *ttg1-24*, show reduced interaction in yeast two-hybrid assays (Long and Schiefelbein, 2020). We therefore studied the interaction of the mutant TTG1 proteins with GL3 in yeast two-hybrid interaction experiments (Figures 2A–2C). We found no interaction between GL3 and the TTG1-1, TTG1-11, and TTG1-12 mutant proteins. The TTG1-9 mutant protein exhibited reduced binding, as judged by weak colony growth. To independently test the protein interaction between GL3 and TTG1 proteins, we studied the interactions using a pull-down assay by expressing the proteins in human embryonic kidney (HEK293TN) cells and a quantification of the precipitated proteins in a luminescence-based mammalian interactome mapping (LUMIER assay; Blasche and

Koegl, 2013). In these experiments, the pull-down efficiencies of the three weak mutant TTG1 proteins and TTG1-1 were ~10-fold lower than wild type but in all experiments clearly significantly above background (*t* test,  $p < 0.001$ ) (Figure 2D). The LUMIER assay appears to be more sensitive and indicate that binding of the mutant TTG1 proteins to GL3 is greatly reduced, but not completely abolished. Also, the binding of the mutant TTG1 proteins to EGL3 and TT8 was impaired in yeast two-hybrid assays (Table S2).

### Nuclear Targeting and Spatial Distribution in the Epidermis of TTG1 Mutant Proteins Is Impaired

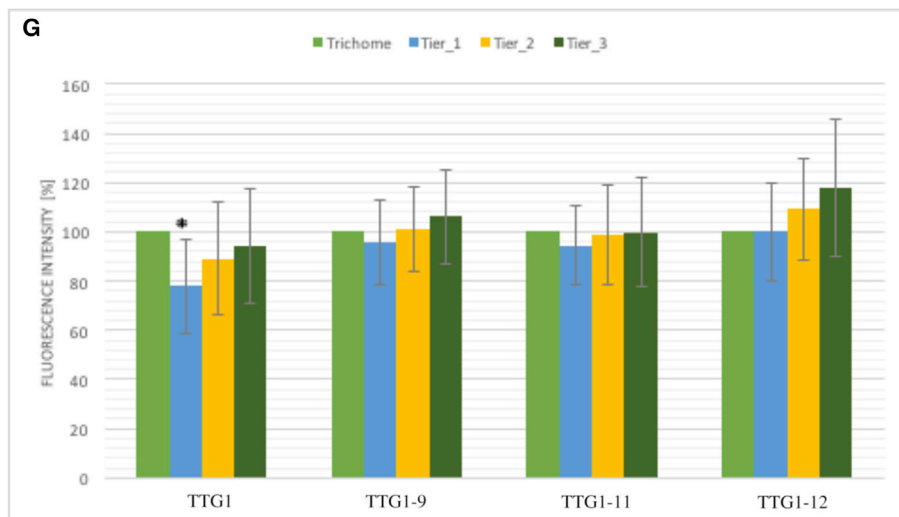
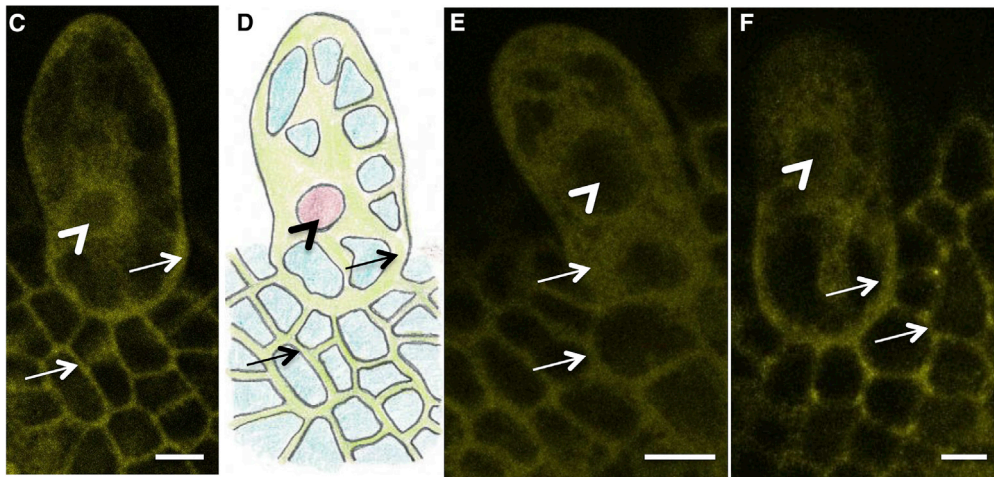
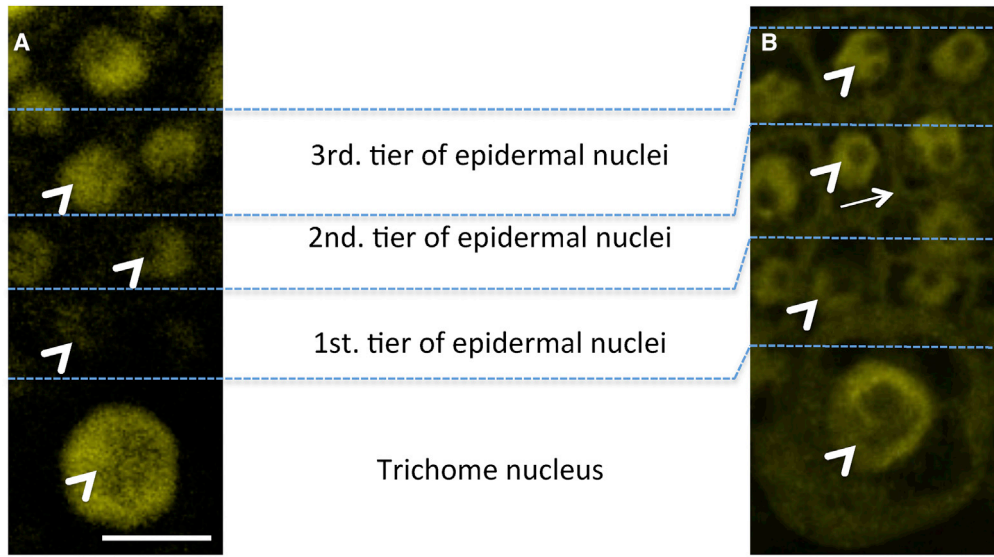
GL3 has been shown to trap TTG1 in the nucleus (Bouyer et al., 2008). We reasoned that the reduced interaction of weak TTG1 mutant proteins with GL3 also affects their nuclear transport. We tested this using the yeast nuclear transportation trap (NTT) assay (Ueki et al., 1998). TTG1 was fused to the transactivator LexAD (LexA DNA-binding domain and GAL4AD transactivation domain) and a nuclear export sequence from HIV Rev protein to generate nuclear export signal (NES)-LexAD-TTG1. The NES sequence mediates nuclear export of TTG1. Binding to GL3 can overcome NES-driven nuclear export, which in turn leads to an activation of the LexAD-responsive *LEUCINE2* gene reporter. Wild-type TTG1 was efficiently targeted to the nucleus (Figures 2E–2G) (Balkunde et al., 2011). By contrast, none of the four TTG1 mutant proteins were directed to the nucleus in these assays (Figures 2E–2G). Thus, the weak binding of mutant TTG1 proteins to GL3 is not sufficient to mediate nuclear transport.

It had been previously shown that wild-type TTG1-YFP protein is localized to the nucleus when expressed in the *ttg1* mutant background (Bouyer et al., 2008). This genetic situation can be considered to reflect the wild-type situation, as two intact TTG1 gene copies are present. To analyze the localization of TTG1-9, TTG1-11, and TTG1-12 proteins in plants, we generated transgenic lines expressing YFP-tagged TTG1 proteins under the control of the *TTG1* promoter. We used the wild-type background to enable the analysis in the context of normal trichome development. TTG1-YFP was localized exclusively in nuclei when expressed in the *ttg1-13* mutant background (Figure 3A; Bouyer et al., 2008). Wild-type TTG1-YFP expressed in wild-type background showed nuclear and cytoplasmic localization (Figure 3B). As this line harbors four TTG1 gene copies, it is conceivable that the increased gene dosage leads to a saturation of the system such that GL3 cannot efficiently target TTG1 to the nucleus anymore (Figure 3B). The three mutant proteins were found predominantly in the cytoplasm, and trichome nuclei had much less fluorescence intensity than the cytoplasm (Figures 3C–3F).

The GL3-dependent localization of TTG1 also results in a depletion of TTG1-YFP in immediate neighbor cells of a developing trichome (39% of the fluorescence found in the trichome)

(D) Pull-down efficiency of TTG1 alleles by ProtA-tagged GL3 in LUMIER assays. The pull-down efficiency of the three weak TTG1 alleles is shown relative to wild type (defined 100%). w/o is the control in which protein extract from non-transformed cells was used.

(E–G) Yeast-based nuclear transportation trap (NTT) assay to test the ability of GL3 to mediate nuclear transport of different TTG1 mutant proteins. (E) Control for presence of plasmids. (F) Nuclear transport assay. Yeast growth indicates GL3-mediated nuclear transport of NES-LexAD-TTG1 proteins. (G) Schematic presentations showing the positions of different combinations on the plates.



(legend on next page)

when expressed in the *ttg1-13* mutant background (Balkunde et al., 2011; Bouyer et al., 2008). The reduced binding or no binding of mutant TTG1 proteins to GL3 suggested to us that they show an altered spatial distribution in the leaf epidermis. As a reference, we show TTG1-YFP expressed in the *ttg1-13* mutant with high levels of fluorescence in the nucleus of the trichome and much lower levels in the epidermal nuclei immediately next to the trichome (Figure 3A, 1st tier; Bouyer et al., 2008). Wild-type plants expressing TTG1-YFP under the TTG1 promoter showed a similar distribution (Figure 3B). In the first tier of cells next to the trichome, TTG1-YFP levels were significantly ( $p = 0.002$ ; Student's *t* test; Table S3) reduced to 78% as compared to the trichome cell, though this depletion is clearly less pronounced as compared to the expression in *ttg1-13* mutants (39%; Bouyer et al., 2008). This is likely due to the difference in the gene dosage in the two experiments. It is conceivable that in this situation, GL3-driven trapping cannot efficiently cope with too much TTG1 protein, leading to reduced depletion. This view is supported by our modeling approach. When simulating different TTG1 levels, we found a decreased depletion for higher TTG1 levels (Figure S3B). In a next step, we analyzed the depletion in the TTG1-9-YFP, TTG1-11-YFP, and TTG1-12-YFP lines. All three lines showed no detectable depletion of the signal in the neighboring epidermal cells (Figures 3C–3G; Table S3). This was consistent with our modeling results simulating the effect of different protein amounts (Figure S3B). Our findings show that the mutant TTG1 proteins are not efficiently targeted to the nucleus and that they do not show the characteristic depletion of TTG1 protein in the immediate neighbor cells.

### Expression of *TRY* and *CPC* in *ttg1* Mutant Alleles

One possibility to explain the cluster phenotype would be that *TRY* is not properly expressed in the weak *ttg1* alleles. Mutations in *TRY* result in the formation of trichome clusters in ~9% of all trichome initiation sites (Schnittger et al., 1999; Szymanski and Marks, 1998). Genetic experiments had suggested that *TRY* and *TTG1* act in the same pathway, as trans-heterozygous mutant combinations show clusters (Schnittger et al., 1999). To test the possibility that the cluster phenotype in weak *ttg1* alleles is due to reduced *TRY* activity by analyzing the expression of *TRY* using a 1.8-kb promoter fragment of *TRY* (*pTRY:GUS*) driving the  $\beta$ -glucuronidase (*GUS*) reporter gene (Pesch and Hülskamp, 2011). In addition, we studied the expression of the *CPC* gene to judge the specificity of regulation events. Here,

we used a 525-bp-long 5' upstream region of the *CPC* gene (*pCPC:GUS*) (Pesch and Hülskamp, 2011).

The *pTRY:GUS* marker was expressed ubiquitously in young wild-type leaves with slightly elevated levels in trichomes (Figure 4A). In mature leaves, *pTRY:GUS* was expressed only in trichomes (Figure 4F). In *ttg1-1*, *ttg1-9*, *ttg1-11*, and *ttg1-12* mutants, we found neither the initial ubiquitous expression on young leaves nor the trichome-specific expression on mature leaves (Figure 4).

The *pCPC:GUS* marker was expressed in trichomes in young and mature leaves (Figures 5A and 5F). The strong *ttg1-13* allele revealed no *CPC* expression (Figures 5E and 5J), and the two weak *ttg1-11* and *ttg1-12* alleles showed clear expression in the few trichomes present on young leaves (Figures 5B–5D and 5G–5I). The expression of *CPC* was not obviously changed in the *ttg1-9* allele (Figures 5B and 5G).

### Rescue of the *ttg1-9* Cluster Phenotype by Expressing *TRY* under the *CPC* Promoter

The expression analysis of *TRY* and *CPC* in weak *ttg1* mutants suggests their differential regulation such that *CPC* is activated while *TRY* is not. If this differential regulation were the reason for the cluster phenotype, then one would expect that the expression of *TRY* under the *CPC* promoter could rescue the cluster phenotype in weak *ttg1* mutants. To test this, we generated transgenic *ttg1-9* lines expressing *TRY* under the control of 525 bp of the 5' upstream region of the *CPC* gene (*pCPC:TRY*; Pesch and Hülskamp, 2011). We analyzed the plants in the T1 generation to statistically cover the whole range of rescue phenotypes (Pesch and Hülskamp, 2011). We observed a general reduction of the trichome number to ~38% of that observed in the single-mutant *ttg1-9* line. This is consistent with the previous observation that *pCPC:TRY* expression in the *try* mutant reduces trichome number (Pesch and Hülskamp, 2011). The cluster frequency was partially rescued. While *ttg1-9* plants exhibit a cluster frequency of 18%, the cluster frequency was significantly reduced to 4.6% in *ttg1-9 pCPC:TRY* plants ( $p < 0.01$ , by Mann-Whitney *U* test; Figure 6; Table S4). *pCPC:TRY* expression in *ttg1-11* and *ttg1-12* alleles did not result in a reduced trichome number (Table S4). However, cluster frequency was significantly reduced in *pCPC:TRY ttg1-11* and *pCPC:TRY ttg1-12* lines. In *ttg1-11 pCPC:TRY*, we found a cluster frequency of 2.8%, while *ttg1-11* showed 7.0% clusters ( $p < 0.01$  by Mann-Whitney *U* test). In *ttg1-12*, cluster frequency was 8.93%, while in *ttg1-12*

### Figure 3. Localization of Wild-Type and Mutant TTG1 Proteins in the Epidermis of *Arabidopsis thaliana*

- (A) TTG1-YFP expressed in *ttg1-13* is localized in the nucleus (arrowhead). High fluorescence is found in the trichome. In 1st-tier nuclei, TTG1-YFP is barely visible, and intensity increases in the 2nd and 3rd tiers.
- (B) TTG1-YFP expressed in wild-type background is found in the cytoplasm (arrows) and the nuclei (arrowhead). Depletion in 1st-tier nuclei is much less pronounced as compared to (A).
- (C) TTG1-9-YFP shows fluorescence in the cytoplasm (arrows) and no or little fluorescence in the nucleus (arrowhead). We found no depletion of fluorescence in the cytoplasm (arrows) of the neighboring cells.
- (D) Color-coded cells shown in (C) to indicate the relevant compartments (red, nucleus; yellow, cytoplasm; blue, vacuole). Epidermal cells contain one large vacuole and a thin cytoplasmic layer at the cortex at this stage of leaf development.
- (E) TTG1-11-YFP.
- (F) TTG1-12-YFP.
- (G) Relative fluorescence intensity in the 1st, 2nd, and 3rd tier of cells as a percentage of the fluorescence measured in the trichome cell in different genetic situations.

Error bars are shown; statistical analysis is shown in Table S3. Scale bars, 10  $\mu$ m.

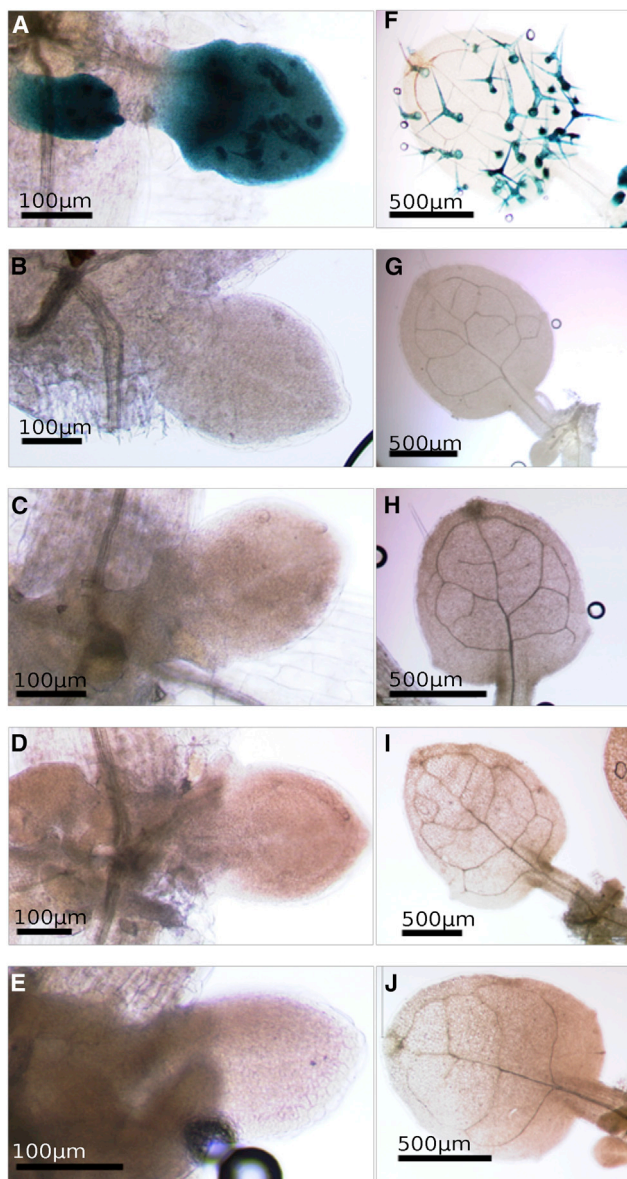


**Figure 4. Expression Pattern of *pTRY:GUS* in Different *ttg1* Alleles**  
(A–J) Left column shows the expression pattern of *pTRY:GUS* in a young leaf (A–E). Right column presents the expression pattern of *pTRY:GUS* in a mature leaf (F–J). (A and F) Col-0. (B and G) *ttg1-9*. (C and H) *ttg1-11*. (D and I) *ttg1-12*. (E and J) *ttg1-13*.

*pCPC:TRY*, cluster formation was significantly reduced to 3.1% (Figure 6). Although we never found a complete rescue, these data indicate that the lack of *TRY* activation in weak *ttg1* alleles causes cluster formation.

#### Mathematical Modeling of TTG1 Dynamics in a Combined AI-AD Model

Weak *ttg1* alleles show three phenotypic aspects: reduced trichome density, strongly enhanced trichome cluster formation, and a seemingly randomized trichome pattern. How are these

three aspects theoretically related? Toward this end, we analyzed hexagonal point patterns (Figure 7A). In a first step, we manipulated a regular hexagonal pattern by randomly perturbing the point coordinates such that the CV of the nearest neighbor distances matched the wild-type pattern (Figure 7B). We assumed that the variation in spacing found in wild-type patterns is the effect of intrinsic fluctuations of cellular processes. These fluctuations result in small cell-to-cell differences in young epidermal tissue, which can have a considerable effect on the final trichome pattern (Greese et al., 2012).

In a second step, we randomly removed points until the density matched the experimentally observed density of *ttg1-9* alleles (Figure 7C). This resulted in an increased variability as measured by the nearest neighbor distribution (CV = 0.65). In a third step, clusters were introduced by moving randomly selected points toward each other, thus forming clusters (Figure 7D). This resulted in a CV matching the *ttg1-9* allele (CV = 0.85), without introducing any additional noise on the resulting point pattern. Thus the pattern of the *ttg1-9* alleles only appears to be more random, and the stochasticity underlying the trichome patterning process is not increased. Therefore, we do not take additional noise sources into account. Rather, as shown by the analysis of these point patterns, the changes of trichome density and clustering are sufficient to explain the full extent of the observed irregularity of the *ttg1-9* phenotype.

To gain mechanistic insight into the role of TTG1 in the patterning network, we derived a minimal combined AI-AD model (Figure 7E, black edges). In this model, TTG1 and GL3 form an active complex (AC). The binding of TTG1 to GL3 leads to a depletion around GL3 maxima. The AC formed by TTG1-GL3 activates both TRY and GL3. Based on the previously published models (Bouyer et al., 2008; Digiuni et al., 2008), we used the following assumptions: (1) TTG1 and TRY are non-cell autonomous (Bouyer et al., 2008; Kurata et al., 2005), and GL3 is cell autonomous (Digiuni et al., 2008). (2) TTG1 and GL3 form the AC (Payne et al., 2000), which activates its own inhibitor, TRY, and has a positive feedback-loop with its activator, GL3 (Digiuni et al., 2008). (3) Inhibition is mediated by TRY binding to GL3 (Digiuni et al., 2008) or the GL3 TTG1 dimer (Pesch et al., 2015). The inhibited complex is explicitly modeled as a dimer (ID) or implicitly as a trimer (IT). (4) Activation of GL3 and TRY by the AC is modeled as activation by two AC units (i.e., a tetramer of TTG1-GL3-GL3-TTG1) (Pesch et al., 2015). This type of non-linearity is a requirement for pattern formation. (5) High concentrations of AC are considered to correspond to trichome cell fate.

The model indicated in black edges in Figure 7E is the simplest combination of AI (Figure 7F) and AD (Figure 7G) patterning motifs and can be reduced to either an AI or AD network by cutting or adding one edge. In particular, adding activation of TTG1 by AC (dashed edge in Figure 7E) yields an AI network similar to previously published AI model (Digiuni et al., 2008) (Figure 7F). Removing the activation of TRY by AC results in the previously published AD model (Bouyer et al., 2008) (Figure 7G). To understand what is gained by the combination of the two motifs, we studied how the two networks shown in Figures 7E–7G perform in explaining the *ttg1-9* phenotype. As the parameters for the

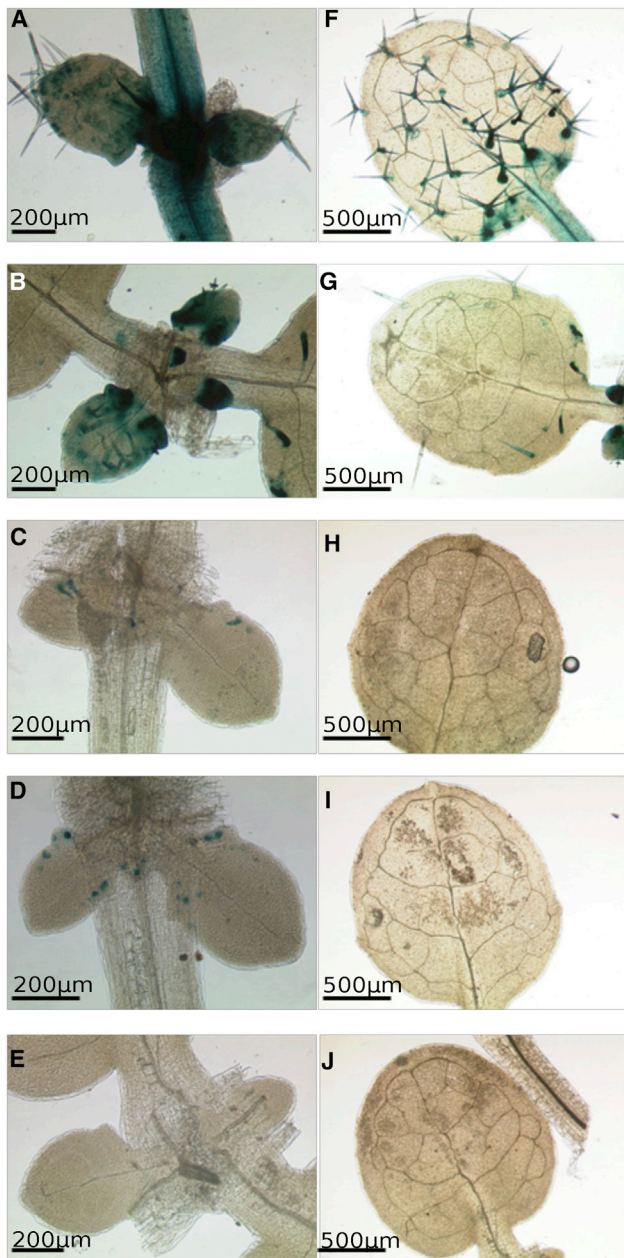


**Figure 5. Expression Pattern of *pCPC:GUS* in Different *ttg1* Alleles**  
(A–J) Left column (A–E) shows the expression pattern of *pCPC:GUS* in a young leaf (A–E). Right column (F–J) shows the expression pattern of *pCPC:GUS* in a mature leaf (F–J). (A and F) Col-0. (B and G) *ttg1-9*. (C and H) *ttg1-11*. (D and I) *ttg1-12*. (E and J) *ttg1-13*.

wild-type network are unknown, we analyzed  $10^6$  randomly generated parameter sets for each model using quasi-Monte-Carlo methods and selected for those able to generate a wild-type pattern defined by the experimentally observed trichome density and zero cluster frequency. Each of those parameter sets constitutes a possible wild-type situation. Next, we analyzed the networks by systematically reducing the binding

strength of TTG1 to GL3 and analyzing the changes in trichome density and cluster frequency.

We investigated the predicted phenotype for the lowest possible TTG1-GL3 binding strength, which still yields a trichome pattern, and compared the values with the experimentally observed *ttg1-9* phenotype. Typically, in the AI model, the reduced binding strength almost never led to the formation of clusters (Figure 7H, blue solid circles). By contrast, the AD model tends to generate too many clusters and a higher trichome density than observed in *ttg1-9* mutants (Figure 7H, gray solid circles). Only the combined model was able to reproduce the experimentally observed trichome density and cluster frequency (Figure 7H, green solid circles). We therefore analyzed the AI-AD model in more detail. To understand how trichome density, cluster frequency, and pattern randomness depend on the interaction strength of TTG1 to GL3, we quantified the three traits for successively decreasing interaction strength (Figure S4). As observed in the *ttg1-9* mutant, decreased interaction strength led to a reduced trichome density ( $0.46 \pm 0.06$ ), an increased apparent randomness (relative CV mutant/wild type =  $2.22 \pm 0.22$ ), and more clustering ( $18\% \pm 7\%$ ).

Next, we analyzed how well the combined model can explain the observed lack of depletion of TTG1-9 in the *ttg1-9* mutants for a range of reduced binding strengths. Unexpectedly, the model predicted a stronger depletion upon a reduction of the binding strength (Figure S4B). This behavior does not depend on a specific parameter set but rather is a generic feature of the AD motif (Figure S5). The failure of the model to reproduce the reduction of depletion can only be overcome by adding additional patterning elements not depending on TTG1. This type of TTG1-independent regulatory event is realistic given that the *ttg1* mutant phenotype can be partially rescued by overexpression of GL3 or EGL3 (Payne et al., 2000; Zhang et al., 2003a).

We therefore included GL1 into the network (Figure 7E, light green edges; Figure S6A). GL1 and GL3 can form an AC, which activates TRY. The interactions included in this sub-part are based on the previously published AI model (Digiuni et al., 2008) (Figure 7F). Similar to the AI model tested in Figure 7H, this model cannot reproduce the cluster formation, however, in contrast to the model without GL1, it is possible to find a reduced depletion of TTG1. The lack of cluster formation is likely due to the activity of TRY, which is maintained throughout different mutation strengths by the GL3-GL1 dimer, thus consistently inhibiting neighboring cells (Figure S6). To overcome this, we introduced the inhibitor CPC (Figure 7E, dark green edges). Through differential dimer formation by TTG1-GL3 and GL1-GL3, we modeled activation of the inhibitors by the different dimers (Figure 7G), where TRY is activated by TTG1-GL3 and CPC by GL1-GL3. This is a simplified form of the competitive binding model suggested before (Pesch et al., 2015). Based on the *cpc* and *try* mutant phenotypes (Hülkamp, 2004; Schellmann et al., 2002) and the finding that CPC is more stable than TRY (Tominaga-Wada and Wada, 2017), we considered CPC to act on long-range distances and TRY to act on short-range distances. Thus, in this model, the loss of TRY through the TTG1 mutation results in a loss of short-range inhibition, whereas CPC is still functioning at long

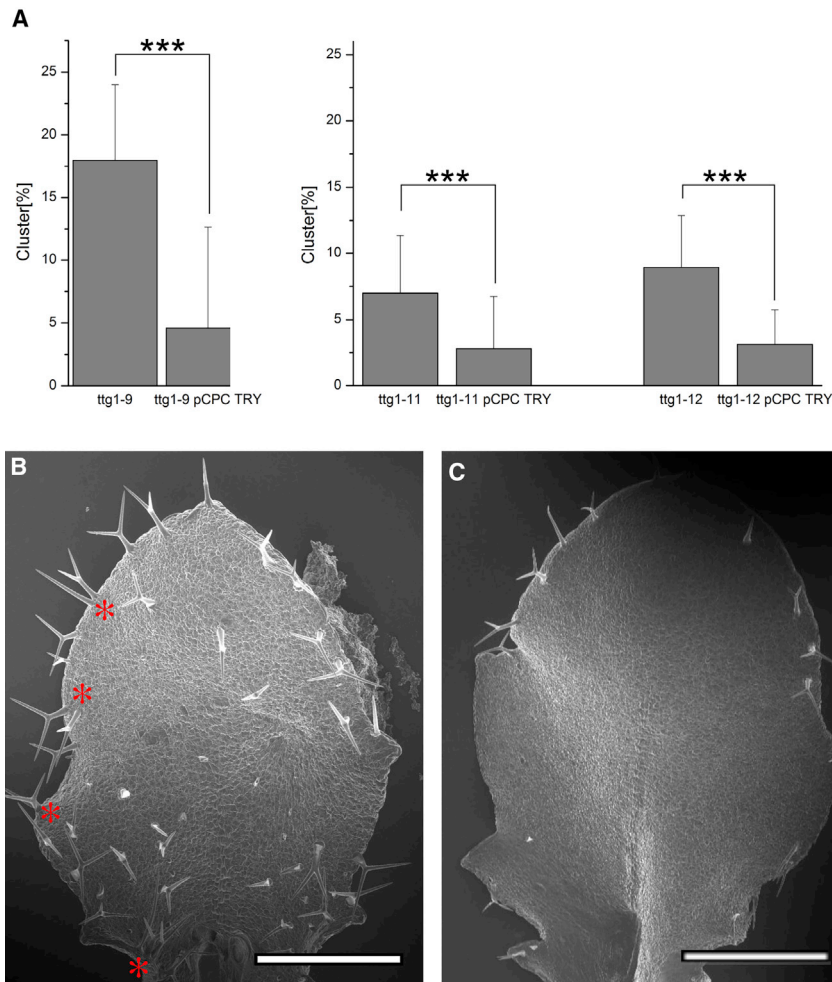


**Figure 6. Rescue of the Cluster Phenotype in Weak *ttg1* Mutants by *pCPC:TRY***

(A) Diagrams showing the cluster frequency in *ttg1* alleles and the respective *pCPC:TRY* rescue lines. Three black asterisk indicate a statistically significant difference between the single mutants and the *pCPC:TRY* rescue lines ( $p < 0.01$ , Wilcoxon test). (B) Representative scanning electron microscope (SEM) image of a young *ttg1-9* plant. Red asterisks indicate the position of trichome clusters. (C) Representative SEM image of a *ttg1-9 pCPC:TRY* plant. Scale bars, 400  $\mu\text{m}$ .

these simulations, we are able to show a partial to full rescue of cluster phenotype based on the change in GL3-GL1-dependent TRY activation (Figures S7C and S7D).

## DISCUSSION

Although it is well established that TTG1 plays a major role in trichome formation in *Arabidopsis thaliana*, its molecular function in trichome patterning remains elusive for at least two reasons. First, because it is a central component in two patterning mechanisms, the AI and AD mechanisms, it is difficult to assess the biological significance in each of them (Pesch and Hülskamp, 2009). Second, competitive complex formation of TTG1-GL3 and GL3-GL1 suggests that TTG1 has different roles in the activation of different MYB-bHLH-WD40 (MBW) target

genes (Pesch et al., 2015). Our analysis of weak *ttg1* alleles sheds some light on both aspects that will be discussed in the following section.

ranges to maintain the trichome pattern. This model is able to predict the changes in trichome density, percentage of trichomes in clusters, and the CV for the nearest neighbor distances for reduced TTG1-GL3 interaction strengths in the same ranges as experimentally observed (Figures 7I–7L). Also, the lower ranges of TTG1-GL3 interaction strength show a reduced amount of depletion compared to wild type. The difference between the inhibitor mobilities is found back in the parameter values used to simulate the *ttg1-9* phenotype (Figure S7A). Further support for this model is found in the analysis of the TTG1 knockout mutant. Our model predicts that the TTG1 knockout is glabrous and can be rescued by overexpression of GL3 (Figures S6C and S6D), which is in line with experimental observations of these mutants (Payne et al., 2000; Zhang et al., 2003a).

Our experimental data show that *TRY* expression is not seen in the *ttg1-9* mutants and indicate that the cluster phenotype can be rescued by trichome-specific expression of *TRY* under the CPC promoter. Consistent with this, our combined AI-AD model predicts a reduced *TRY* expression when the interaction strength of TTG1 to GL3 is reduced (Figure S7B). We also simulated the *ttg1-9 pCPC:TRY* rescue experiment by varying the parameters for the activation of *TRY* by the GL3-GL1 dimer. In

genes (Pesch et al., 2015). Our analysis of weak *ttg1* alleles sheds some light on both aspects that will be discussed in the following section.

### Regulation of *TRY* by *TTG1*

The analysis of genetic interactions between *TRY* and *TTG1* suggested a regulation of *TRY* by *TTG1* (Schnittger et al., 1999). Various *try/+ ttg1/+* double-heterozygous combinations of *try* and different *ttg1* null-alleles exhibited clusters. Thus, the reduced activity of both genes is sufficient to cause a phenotypic effect indicating that they act in the same pathway. Recent molecular data suggest that TTG1 regulates MBW target genes, including *TRY*, in a differential manner in the root hair system (Long and Schiefelbein, 2020). One possible molecular explanation is the competitive complex formation of the MBW complex. It was reported that the activation of the *TRY* promoter by TTG1 and GL3 is counteracted by GL1, whereas GL3-GL1-dependent activation of the *CPC* promoter is repressed by TTG1 (Pesch et al., 2015). Consistent with the regulation scheme, we observed a differential regulation of *TRY* and *CPC* in weak *ttg1* alleles. Our data can explain the observed lack of *TRY* activation in weak *ttg1* alleles by two related causes: (1) the interaction

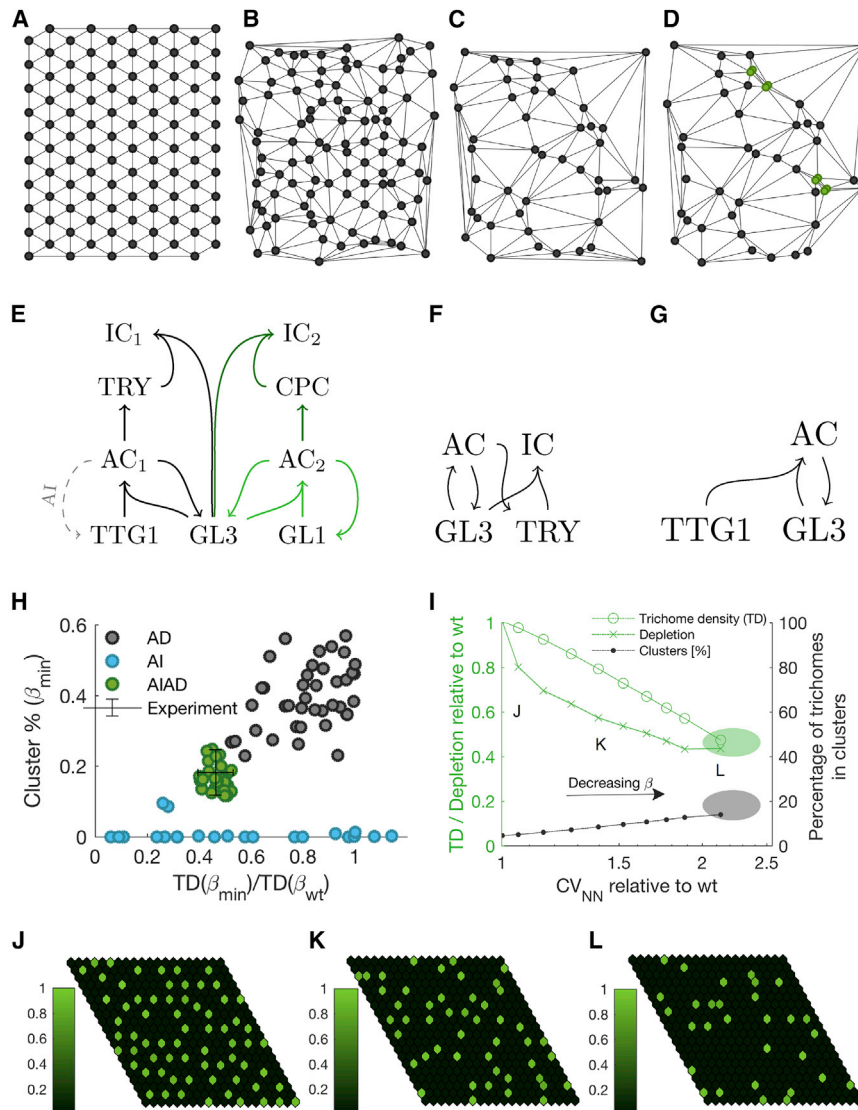


**Figure 7. Analysis of Point Patterns and Development of Trichome Model Networks**

(A–D) Distribution of points on hexagonal grid. Lines between points are edges determined by Delaunay triangulation and indicate connectivity between points. Starting from a completely regular point distribution (A), point coordinates are perturbed (B), randomly removed (C), and clustered (D) (clusters indicated in green). The pattern in (D) represents a typical *ttg1-9* leaf.

(E–G) Interaction scheme of the combined activator-inhibitor (AI) activator-depletion (AD) (AI-AD) model (E), the AI model (F), and the AD model (G). The dashed, gray edge in (E) indicates an additional feedback that can be used to convert the AI-AD to an AI-type network. TTG1 and GL3 form an active complex (AC) that activates TRY. In turn, TRY binds to GL3, thus forming an inactive complex (IC). The colors in (E) indicate the different additions needed to explain the *ttg1-9* phenotype. The black edges indicate the simplest form of the combination of the networks in (F) and (G). Light green indicates the edges needed for including GL1, and dark green edges are added upon CPC inclusion. For simplicity, basal production, degradation, and diffusion are not indicated.

(H) Comparison of the AI (blue), AD (gray), and AI-AD (green) models. Each point is a different parameter set tested for the *ttg1-9* phenotype. The trichome densities are relative to wild type, where  $\beta_{min}$  is the strongest possible mutation for the TTG1-GL3 interaction parameter and  $\beta_{wt}$  is the value for the wild-type simulation.

(I) Each point on the lines indicates a different relative change in binding strength ( $\beta$ ) and the mean effect this has on the pattern in terms of relative trichome density (left y axis, circles), depletion (left y axis, crosses), percentage of clusters (right y axis), and coefficient of variation (CV) in nearest neighbor distances (x axis). From the leftmost point in the plot to the rightmost point, the TTG1-GL3 interaction is decreased, as indicated by the arrow. The green and gray shaded area indicates experimental data ranges for trichome density and cluster percentages on *ttg1-9* leaves, respectively. A shaded line indicates the 95% confidence interval determined by bootstrapping of a varying number of simulations; note that this area is smaller than the line width. The letters J, K, and L in the plot correspond to example simulations given below the plot.

(legend continued on next page)

between mutant TTG1 and GL3 is reduced, and (2) the binding of GL1 to GL3 is not counteracted by mutant TTG1.

### Role of TTG1 in the AD Scenario

The AD model for trichome patterning is based on three experimental datasets: the interaction of TTG1 with GL3, the nuclear targeting of TTG1 by GL3, and the lack of depletion in the cells immediately next to incipient trichomes (Balkunde et al., 2011; Bouyer et al., 2008). We show that all three aspects are impaired in weak *ttg1* alleles. Thus, by all criteria, the AD mechanism is not operating in these alleles. This raises the question of whether the randomization of the trichome pattern in weak *ttg1* alleles is caused by the lack of the AD mechanism. This is difficult to answer, as it is not clear whether and to what extent the AI mechanism is still operating. The mutual competition of TTG1 and GL1 for binding to GL3 (Pesch et al., 2015) suggests that TTG1 GL3 and GL3 GL1 can act separately to transcriptionally activate inhibitory patterning genes. In this light, one could postulate that GL3, GL1, and CPC can still function as an AI unit in weak *ttg1* alleles. In fact, the results from the mathematical modeling suggest that GL3, GL1, and CPC are necessary to reproduce all observations.

### Is the Reduced Interaction of TTG1 Mutant Protein with GL3 Sufficient to Explain the *ttg1* Trichome Phenotypes?

When reducing the TTG1-GL3 interaction strength in the AI-AD model, we can robustly reproduce the patterning defects, indicating that the proposed AI-AD model is sufficient to explain the full spectrum of trichome defects in strong and weak *ttg1* mutants. A reduction of TTG1-GL3 interactions is predicted to cause reduced AC levels. This, in turn, leads to a lower activation of TRY. The reduced activation of TRY explains the increased cluster frequency.

One aspect that cannot be matched by the simplest form of the model (black edges in Figure 7E) is the loss of depletion in the *ttg1* mutants. This stems from the characteristics of the AD sub-motif. The reduction in TTG1-GL3 interaction results in a focusing effect of TTG1, which counteracts a loss of depletion. This characteristic persists in the combined AI-AD model and suggests that TTG1-independent regulation aspects are missing from the network. After the inclusion of GL1 into the model, we can find reduction of depletion as a result of reduced TTG1-GL3 interaction; however, clusters are not formed in this model. Ultimately, the differential regulation of the inhibitors CPC and TRY was needed to find loss of depletion in combination with the patterning defects found for the *ttg1-9* allele. Here, two main requirements needed to be fulfilled. First, an additional motif needed to be introduced that could pattern independently of TTG1, and this was achieved through the inclusion of GL1 (black and light green edges in Figure 7E). This second patterning mechanism increases pattern-forming robustness against the TTG1 mutation, resulting in a pattern that is not

dependent on the depletion of TTG1 at its core. A model without GL1 would always need TTG1 depletion as a basis for forming a pattern (Figure S5). Second, CPC was introduced under the regulation of GL1-GL3 (complete network in Figure 7E). Without CPC, GL3-GL1 would still activate TRY despite changes in the TTG1 GL3 interaction strength, thereby maintaining high levels of TRY such that no clusters are formed (Figure S6B). Now, with the addition of CPC and differential dimer regulation, the reduction in TTG1-GL3 interaction leads to a reduced amount of TRY in the system, resulting in clusters. Furthermore, from the selected randomly generated parameter sets, we find that TRY operates on shorter ranges than CPC (Figure S7A). This relatively short-range radius of effect ensures that clusters are formed when the reduction in TTG1-GL3 interaction strength results in reduced amounts of TRY.

We combined the AI and AD spatial patterning motifs to explain a complex patterning phenotype as a result of a point mutation. To overcome the challenge of incomplete information about the system parameters, we adopted a constraint global analysis method using a quasi-Monte Carlo approach. For every randomly chosen parameter set, the model had to first reproduce the observed wild-type pattern and subsequently replicate the complex mutant phenotype. This approach revealed that neither the AI motif nor the AD motif is structurally capable of explaining the observed data. Moreover, by seeking for a minimal model, our approach disclosed that the combination of the AD and AI motifs plus an extension by an extra inhibitor is required to capture the observations. Our combined and extended AI-AD model provides a link between genotype and phenotype and offers a consistent explanation how a point mutation can result into reduced trichome density and increased cluster frequency at the same time.

### STAR★METHODS

Detailed methods are provided in the online version of this paper and include the following:

- KEY RESOURCES TABLE
- RESOURCE AVAILABILITY
  - Lead contact
  - Materials availability
  - Data and code availability
- EXPERIMENTAL MODEL AND SUBJECT DETAILS
- METHOD DETAILS
  - Analysis of fluorescence intensity in trichomes and surrounding tiers
  - Light microscopy
  - Yeast two hybrid and nuclear transport assays
  - LUMIER
  - Constructs
  - Generation of a random pattern
  - Quantification of the regularity of patterns

(J) Example simulation of a wild-type situation.

(K) Example simulation that resembles the wild-type situation. In this simulation, the binding between TTG1 and GL3 is decreased, but not to such an extent that it replicates *ttg1-9* phenotypes.

(L) An example of a *ttg1-9* simulation. In this case, the pattern shows clusters, reduced density, and irregularity, in the same relative quantities as observed experimentally.

- Theoretical probability of finding clusters in random patterns
  - Correlation dimension of experimental data and simulated patterns
  - Reproducing trichome pattern irregularity by perturbing hexagonal patterns
  - Trichome patterning model
  - Pattern quantification
  - Parameter scan
  - Parameter criteria
  - Depletion in the activator-depletion model
  - Dispersion relation
- **QUANTIFICATION AND STATISTICAL ANALYSIS**

#### SUPPLEMENTAL INFORMATION

Supplemental Information can be found online at <https://doi.org/10.1016/j.celrep.2020.108497>.

#### ACKNOWLEDGMENTS

We would like to thank Birgit Kernebeck, Sabine Lohmer, and Irene Klinkhammer for excellent experimental help. This work was funded by the DFG priority program SFB 572. R.B. was supported by the International Graduate School in Genetics and Functional Genomics, and B.J. was supported by the IMPRS: International Max Planck Research School at the MPIZ for Plant Breeding Research.

#### AUTHOR CONTRIBUTIONS

R.B., H.B., B.Z., S.H., B.J., and M.P. performed the experiments and analyzed the data. A.D. and C.F. did the mathematical modeling and analysis. M.H. supervised the experiments. M.H., A.D., and C.F. wrote the manuscript.

#### DECLARATION OF INTERESTS

The authors declare no competing interests.

Received: November 9, 2018  
Revised: September 2, 2020  
Accepted: November 18, 2020  
Published: December 15, 2020

#### REFERENCES

Balkunde, R., Pesch, M., and Hülskamp, M. (2010). Trichome patterning in *Arabidopsis thaliana* from genetic to molecular models. *Curr. Top. Dev. Biol.* *91*, 299–321.

Balkunde, R., Bouyer, D., and Hülskamp, M. (2011). Nuclear trapping by GL3 controls intercellular transport and redistribution of TTG1 protein in *Arabidopsis*. *Development* *138*, 5039–5048.

Benitez, M., Espinosa-Soto, C., Padilla-Longoria, P., Diaz, J., and Alvarez-Buylla, E.R. (2007). Equivalent genetic regulatory networks in different contexts recover contrasting spatial cell patterns that resemble those in *Arabidopsis* root and leaf epidermis: a dynamic model. *Int. J. Dev. Biol.* *51*, 139–155.

Benitez, M., Espinosa-Soto, C., Padilla-Longoria, P., and Alvarez-Buylla, E.R. (2008). Interlinked nonlinear subnetworks underlie the formation of robust cellular patterns in *Arabidopsis* epidermis: a dynamic spatial model. *BMC Syst. Biol.* *2*, 98.

Bernhardt, C., Lee, M.M., Gonzalez, A., Zhang, F., Lloyd, A., and Schiefelbein, J. (2003). The bHLH genes *GLABRA3* (GL3) and *ENHANCER OF GLABRA3* (EGL3) specify epidermal cell fate in the *Arabidopsis* root. *Development* *130*, 6431–6439.

Blasche, S., and Koegl, M. (2013). Analysis of protein-protein interactions using LUMIER assays. *Methods Mol. Biol.* *1064*, 17–27.

Bouyer, D., Geier, F., Kragler, F., Schnittger, A., Pesch, M., Wester, K., Balkunde, R., Timmer, J., Fleck, C., and Hülskamp, M. (2008). Two-dimensional patterning by a trapping/depletion mechanism: the role of TTG1 and GL3 in *Arabidopsis* trichome formation. *PLoS Biol.* *6*, e141.

Clough, S.J., and Bent, A.F. (1998). Floral dip: a simplified method for *Agrobacterium*-mediated transformation of *Arabidopsis thaliana*. *Plant J.* *16*, 735–743.

Digiuni, S., Schellmann, S., Geier, F., Greese, B., Pesch, M., Wester, K., Dantan, B., Mach, V., Srinivas, B.P., Timmer, J., et al. (2008). A competitive complex formation mechanism underlies trichome patterning on *Arabidopsis* leaves. *Mol. Syst. Biol.* *4*, 217.

Esch, J.J., Chen, M., Sanders, M., Hillestad, M., Ndkium, S., Idelkope, B., Neizer, J., and Marks, M.D. (2003). A contradictory *GLABRA3* allele helps define gene interactions controlling trichome development in *Arabidopsis*. *Development* *130*, 5885–5894.

Failmezger, H., Jaegle, B., Schrader, A., Hülskamp, M., and Tresch, A. (2013). Semi-automated 3D leaf reconstruction and analysis of trichome patterning from light microscopic images. *PLoS Comput. Biol.* *9*, e1003029.

Galway, M.E., Masucci, J.D., Lloyd, A.M., Walbot, V., Davis, R.W., and Schiefelbein, J.W. (1994). The TTG gene is required to specify epidermal cell fate and cell patterning in the *Arabidopsis* root. *Dev. Biol.* *166*, 740–754.

Gan, L., Xia, K., Chen, J.G., and Wang, S. (2011). Functional characterization of *TRICHOMELESS2*, a new single-repeat R3 MYB transcription factor in the regulation of trichome patterning in *Arabidopsis*. *BMC Plant Biol.* *11*, 176.

Gao, Y., Gong, X., Cao, W., Zhao, J., Fu, L., Wang, X., Schumaker, K.S., and Guo, Y. (2008). *SAD2* in *Arabidopsis* functions in trichome initiation through mediating GL3 function and regulating GL1, TTG1 and GL2 expression. *J. Integr. Plant Biol.* *50*, 906–917.

Gietz, R.D., Schiestl, R.H., Willems, A.R., and Woods, R.A. (1995). Studies on the transformation of intact yeast cells by the LiAc/SS-DNA/PEG procedure. *Yeast* *11*, 355–360.

Grassberger, P., and Procaccia, I. (1983). Characterization of strange attractors. *Phys. Rev. Lett.* *50*, 346.

Grebe, M. (2012). The patterning of epidermal hairs in *Arabidopsis*—updated. *Curr. Opin. Plant Biol.* *15*, 31–37.

Greese, B., Wester, K., Bensch, R., Ronneberger, O., Timmer, J., Huelskamp, M., and Fleck, C. (2012). Influence of cell-to-cell variability on spatial pattern formation. *IET Syst. Biol.* *6*, 143–153.

Hanahan, D. (1983). Studies on transformation of *Escherichia coli* with plasmids. *J. Mol. Biol.* *166*, 557–580.

Holgate, P. (1965). Tests of randomness based on distance methods. *Biometrika* *52*, 345–353.

Hülskamp, M. (2004). Plant trichomes: a model for cell differentiation. *Nat. Rev. Mol. Cell Biol.* *5*, 471–480.

Hülskamp, M., Misra, S., and Jürgens, G. (1994). Genetic dissection of trichome cell development in *Arabidopsis*. *Cell* *76*, 555–566.

James, P., Halladay, J., and Craig, E.A. (1996). Genomic libraries and a host strain designed for highly efficient two-hybrid selection in yeast. *Genetics* *144*, 1425–1436.

Kirik, V., Schnittger, A., Radchuk, V., Adler, K., Hülskamp, M., and Bäumllein, H. (2001). Ectopic expression of the *Arabidopsis* *AtMYB23* gene induces differentiation of trichome cells. *Dev. Biol.* *235*, 366–377.

Kirik, V., Simon, M., Huelskamp, M., and Schiefelbein, J. (2004a). The *ENHANCER OF TRY AND CPC1* gene acts redundantly with *TRIPTYCHON* and *CAPRICE* in trichome and root hair cell patterning in *Arabidopsis*. *Dev. Biol.* *268*, 506–513.

Kirik, V., Simon, M., Wester, K., Schiefelbein, J., and Hülskamp, M. (2004b). *ENHANCER OF TRY AND CPC 2 (ETC2)* reveals redundancy in the region-specific control of trichome development of *Arabidopsis*. *Plant Mol. Biol.* *55*, 389–398.

- Kirik, V., Lee, M.M., Wester, K., Herrmann, U., Zheng, Z., Oppenheimer, D., Schiefelbein, J., and Hülskamp, M. (2005a). Functional diversification of MYB23 and GL1 genes in trichome morphogenesis and initiation. *Development* **132**, 1477–1485.
- Kirik, V., Lee, M.M., Wester, K., Herrmann, U., Zheng, Z.G., Oppenheimer, D., Schiefelbein, J., and Hülskamp, M. (2005b). Functional diversification of MYB23 and GL1 genes in trichome morphogenesis and initiation. *Development* **132**, 1749.
- Koornneef, M. (1981). The complex syndrome of *ttg* mutants. *Arabidopsis Information Service* **18**, 45–51.
- Koornneef, M., Dellaert, L.W., and van der Veen, J.H. (1982). EMS- and radiation-induced mutation frequencies at individual loci in *Arabidopsis thaliana* (L.) Heynh. *Mutat. Res.* **93**, 109–123.
- Kurata, T., Ishida, T., Kawabata-Awai, C., Noguchi, M., Hattori, S., Sano, R., Nagasaka, R., Tominaga, R., Koshino-Kimura, Y., Kato, T., et al. (2005). Cell-to-cell movement of the CAPRICE protein in *Arabidopsis* root epidermal cell differentiation. *Development* **132**, 5387–5398.
- Larkin, J.C., Oppenheimer, D.G., Lloyd, A.M., Paparozzi, E.T., and Marks, M.D. (1994). Roles of the GLABROUS1 and TRANSPARENT TESTA GLABRA Genes in *Arabidopsis* Trichome Development. *Plant Cell* **6**, 1065–1076.
- Larkin, J.C., Walker, J.D., Bolognesi-Winfield, A.C., Gray, J.C., and Walker, A.R. (1999). Allele-specific interactions between *ttg* and *gl1* during trichome development in *Arabidopsis thaliana*. *Genetics* **151**, 1591–1604.
- Long, Y., and Schiefelbein, J. (2020). Novel *TTG1* mutants modify root-hair pattern formation in *Arabidopsis*. *Front. Plant Sci.* **11**, 383.
- Meinhardt, H., and Gierer, A. (1974). Applications of a theory of biological pattern formation based on lateral inhibition. *J. Cell Sci.* **15**, 321–346.
- Murray, J.D. (2002). *Mathematical Biology I: An Introduction*. Interdisciplinary Applied Mathematics 17 (Springer Verlag).
- Oppenheimer, D.G., Herman, P.L., Sivakumaran, S., Esch, J., and Marks, M.D. (1991). A myb gene required for leaf trichome differentiation in *Arabidopsis* is expressed in stipules. *Cell* **67**, 483–493.
- Payne, C.T., Zhang, F., and Lloyd, A.M. (2000). GL3 encodes a bHLH protein that regulates trichome development in *Arabidopsis* through interaction with GL1 and TTG1. *Genetics* **156**, 1349–1362.
- Pesch, M., and Hülskamp, M. (2004). Creating a two-dimensional pattern de novo during *Arabidopsis* trichome and root hair initiation. *Curr. Opin. Genet. Dev.* **14**, 422–427.
- Pesch, M., and Hülskamp, M. (2009). One, two, three...models for trichome patterning in *Arabidopsis*? *Curr. Opin. Plant Biol.* **12**, 587–592.
- Pesch, M., and Hülskamp, M. (2011). Role of TRIPTYCHON in trichome patterning in *Arabidopsis*. *BMC Plant Biol.* **11**, 130.
- Pesch, M., Schultheiß, I., Digiuni, S., Uhrig, J.F., and Hülskamp, M. (2013). Mutual control of intracellular localisation of the patterning proteins AtMYC1, GL1 and TRY/CPC in *Arabidopsis*. *Development* **140**, 3456–3467.
- Pesch, M., Schultheiß, I., Klopffleisch, K., Uhrig, J.F., Koegl, M., Clemen, C.S., Simon, R., Weidtkamp-Peters, S., and Hülskamp, M. (2015). TRANSPARENT TESTA GLABRA1 and GLABRA1 Compete for Binding to GLABRA3 in *Arabidopsis*. *Plant Physiol.* **168**, 584–597.
- Sandler, O., Mizrahi, S.P., Weiss, N., Agam, O., Simon, I., and Balaban, N.Q. (2015). Lineage correlations of single cell division time as a probe of cell-cycle dynamics. *Nature* **519**, 468–471.
- Schellmann, S., Schnittger, A., Kirik, V., Wada, T., Okada, K., Beermann, A., Thumfahrt, J., Jürgens, G., and Hülskamp, M. (2002). TRIPTYCHON and CAPRICE mediate lateral inhibition during trichome and root hair patterning in *Arabidopsis*. *EMBO J.* **21**, 5036–5046.
- Schnittger, A., Folkers, U., Schwab, B., Jürgens, G., and Hülskamp, M. (1999). Generation of a spacing pattern: the role of triptychon in trichome patterning in *Arabidopsis*. *Plant Cell* **11**, 1105–1116.
- Sessions, A., Weigel, D., and Yanofsky, M.F. (1999). The *Arabidopsis thaliana* MERISTEM LAYER 1 promoter specifies epidermal expression in meristems and young primordia. *Plant J.* **20**, 259–263.
- Skinner, J.E. (1994). Low-dimensional chaos in biological systems. *Biotechnology (N. Y.)* **12**, 596–600.
- Szymanski, D.B., and Marks, M.D. (1998). GLABROUS1 overexpression and TRIPTYCHON alter the cell cycle and trichome cell fate in *Arabidopsis*. *Plant Cell* **10**, 2047–2062.
- Theiler, J. (1987). Efficient algorithm for estimating the correlation dimension from a set of discrete points. *Phys. Rev. A Gen. Physiol.* **36**, 4456–4462.
- Tominaga, R., Iwata, M., Sano, R., Inoue, K., Okada, K., and Wada, T. (2008). *Arabidopsis* CAPRICE-LIKE MYB 3 (CPL3) controls endoreduplication and flowering development in addition to trichome and root hair formation. *Development* **135**, 1335–1345.
- Tominaga-Wada, R., and Wada, T. (2017). Extended C termini of CPC-LIKE MYB proteins confer functional diversity in *Arabidopsis* epidermal cell differentiation. *Development* **144**, 2375–2380.
- Tominaga-Wada, R., Ishida, T., and Wada, T. (2011). New insights into the mechanism of development of *Arabidopsis* root hairs and trichomes. *Int. Rev. Cell Mol. Biol.* **286**, 67–106.
- Turing, A. (1952). The chemical basis of morphogenesis. *Philos. Trans. R. Soc. Lond. B Biol. Sci.* **237**, 37–72.
- Ueki, N., Oda, T., Kondo, M., Yano, K., Noguchi, T., and Muramatsu, M. (1998). Selection system for genes encoding nuclear-targeted proteins. *Nat. Biotechnol.* **16**, 1338–1342.
- Wada, T., Tachibana, T., Shimura, Y., and Okada, K. (1997). Epidermal cell differentiation in *Arabidopsis* determined by a Myb homolog, CPC. *Science* **277**, 1113–1116.
- Walker, A.R., Davison, P.A., Bolognesi-Winfield, A.C., James, C.M., Srinivasan, N., Blundell, T.L., Esch, J.J., Marks, M.D., and Gray, J.C. (1999). The TRANSPARENT TESTA GLABRA1 locus, which regulates trichome differentiation and anthocyanin biosynthesis in *Arabidopsis*, encodes a WD40 repeat protein. *Plant Cell* **11**, 1337–1350.
- Wang, S., and Chen, J.G. (2008). *Arabidopsis* transient expression analysis reveals that activation of GLABRA2 may require concurrent binding of GLABRA1 and GLABRA3 to the promoter of GLABRA2. *Plant Cell Physiol.* **49**, 1792–1804.
- Wang, S., Kwak, S.H., Zeng, Q., Ellis, B.E., Chen, X.Y., Schiefelbein, J., and Chen, J.G. (2007). TRICHOMELESS1 regulates trichome patterning by suppressing GLABRA1 in *Arabidopsis*. *Development* **134**, 3873–3882.
- Wang, S., Hubbard, L., Chang, Y., Guo, J., Schiefelbein, J., and Chen, J.G. (2008). Comprehensive analysis of single-repeat R3 MYB proteins in epidermal cell patterning and their transcriptional regulation in *Arabidopsis*. *BMC Plant Biol.* **8**, 81.
- Wang, S., Barron, C., Schiefelbein, J., and Chen, J.G. (2010). Distinct relationships between GLABRA2 and single-repeat R3 MYB transcription factors in the regulation of trichome and root hair patterning in *Arabidopsis*. *New Phytol.* **185**, 387–400.
- Wester, K., Digiuni, S., Geier, F., Timmer, J., Fleck, C., and Hülskamp, M. (2009). Functional diversity of R3 single-repeat genes in trichome development. *Development* **136**, 1487–1496.
- Western, T.L., Skinner, D.J., and Haughn, G.W. (2000). Differentiation of mucilage secretory cells of the *Arabidopsis* seed coat. *Plant Physiol.* **122**, 345–356.
- Zhang, F., Gonzalez, A., Zhao, M., Payne, C.T., and Lloyd, A. (2003a). A network of redundant bHLH proteins functions in all TTG1-dependent pathways of *Arabidopsis*. *Development* **130**, 4859–4869.
- Zhao, M., Morohashi, K., Hatlestad, G., Grotewold, E., and Lloyd, A. (2008). The TTG1-bHLH-MYB complex controls trichome cell fate and patterning through direct targeting of regulatory loci. *Development* **135**, 1991–1999.
- Zimmermann, I.M., Heim, M.A., Weisshaar, B., and Uhrig, J.F. (2004). Comprehensive identification of *Arabidopsis thaliana* MYB transcription factors interacting with R/B-like BHLH proteins. *Plant J.* **40**, 22–34.

STAR★METHODS

KEY RESOURCES TABLE

REAGENT or RESOURCE	SOURCE	IDENTIFIER
Bacterial and Virus Strains		
<i>E. coli</i> DH5 $\alpha$	<a href="#">Hanahan, 1983</a>	
<i>E. coli</i> DB3.1	Invitrogen	
Chemicals, Peptides, and Recombinant Proteins		
Ruthenium Red	Sigma	84071
X-Gluc	Sigma	70036-M
Experimental Models: Cell Lines		
HEK293TN cells	BioCat/SBI	LV900A-1
Experimental Models: Organisms/Strains		
<i>Arabidopsis thaliana</i> (Col-0)	Maarten Koornneef	
<i>Arabidopsis thaliana</i> <i>ttg1-1</i>	<a href="#">Koornneef, 1981</a>	
<i>Arabidopsis thaliana</i> <i>ttg1-9</i>	<a href="#">Larkin et al., 1994</a> ; <a href="#">Walker et al., 1999</a>	
<i>Arabidopsis thaliana</i> <i>ttg1-11</i>	<a href="#">Larkin et al., 1994, 1999</a>	
<i>Arabidopsis thaliana</i> <i>ttg1-12</i>	<a href="#">Larkin et al., 1994, 1999</a>	
<i>Arabidopsis thaliana</i> <i>ttg1-13</i>	<a href="#">Larkin et al., 1999</a>	
<i>Arabidopsis thaliana</i> <i>ttg1-13</i> pTTG1:TTG1-YFP	This study	
<i>Arabidopsis thaliana</i> (Col-0) pTTG1:TTG1-YFP	This study	
<i>Arabidopsis thaliana</i> (Col-0) pTTG1:TTG1-9-YFP	This study	
<i>Arabidopsis thaliana</i> (Col-0) pTTG1:TTG1-11-YFP	This study	
<i>Arabidopsis thaliana</i> (Col-0) pTTG1:TTG1-12-YFP	This study	
<i>Arabidopsis thaliana</i> <i>ttg1-9</i> pCPC:TRY	This study	
<i>Arabidopsis thaliana</i> <i>ttg1-11</i> pCPC:TRY	This study	
<i>Arabidopsis thaliana</i> <i>ttg1-12</i> pCPC:TRY	This study	
<i>Arabidopsis thaliana</i> (Col-0) pCPC:GUS	This study	
<i>Arabidopsis thaliana</i> <i>ttg1-13</i> pCPC:GUS	This study	
<i>Arabidopsis thaliana</i> <i>ttg1-9</i> pCPC:GUS	This study	
<i>Arabidopsis thaliana</i> <i>ttg1-11</i> pCPC:GUS	This study	
<i>Arabidopsis thaliana</i> <i>ttg1-12</i> pCPC:GUS	This study	
<i>Arabidopsis thaliana</i> (Col-0) pTRY:GUS	This study	
<i>Arabidopsis thaliana</i> <i>ttg1-13</i> pTRY:GUS	This study	
<i>Arabidopsis thaliana</i> <i>ttg1-9</i> pTRY:GUS	This study	
<i>Arabidopsis thaliana</i> <i>ttg1-11</i> pTRY:GUS	This study	
<i>Arabidopsis thaliana</i> <i>ttg1-12</i> pTRY:GUS	This study	
<i>Saccharomyces cerevisiae</i> strain AH109	<a href="#">James et al., 1996</a>	
<i>Saccharomyces cerevisiae</i> strain EGY48	<a href="#">Ueki et al., 1998</a>	
Oligonucleotides		
RB-TTG1 ( <i>ttg1-11</i> G149R) Fwd	Sigma-Aldrich	
CTCAGAACTTGTAGTATTGATACGAC		

(Continued on next page)

**Continued**

REAGENT or RESOURCE	SOURCE	IDENTIFIER
RB-TTG1 (ttg1-11 G149R) Rev ACGTTTCGGCTCTACATCGTTC	Sigma-Aldrich	
RB-TTG1 (ttg1-12 G43R) Fwd GCCGTCAGAAGCTTCCTCGAAG	Sigma-Aldrich	
RB-TTG1 (ttg1-12 G43R) Rev GATTCTGTGACCGGAGGATGAGCG	Sigma-Aldrich	
RB-TTG1-S282F-Fwd ATTTGTTTTGGTGGTGATGATACACA	Sigma-Aldrich	
RB-TTG1-Int 279-Rev ATGTTTACAGCTCTGAGGCGCC	Sigma-Aldrich	
Recombinant DNA		
pTTG1:TTG1-YFP (pAMPAT)	This study	
pTTG1:TTG1-9-YFP (pAMPAT)	This study	
pTTG1:TTG1-11-YFP (pAMPAT)	This study	
pTTG1:TTG1-12-YFP (pAMPAT)	This study	
pNS-TTG1	<a href="#">Balkunde et al., 2011</a>	
pVT-U-GL3	<a href="#">Balkunde et al., 2011</a>	
pNS-TTG1-13	<a href="#">Balkunde et al., 2011</a>	
pNS-TTG1-9	This study	
pNS-TTG1-11	This study	
pNS-TTG1-12	This study	
pAS2-TTG1	This study	
pAS2-TTG1-13	This study	
pAS2-TTG1-9	This study	
pAS2-TTG1-11	This study	
pAS2-TTG1-12	This study	
pC-ACT2-GL3	This study	
pC-ACT2-EGL3	This study	
pC-ACT2-TT8	This study	
Software and Algorithms		
ImageJ	Fabrice Cordelieres, Institut Curie, Orsay, France	<a href="https://imagej.nih.gov/ij/">https://imagej.nih.gov/ij/</a>
MATLAB, 2016. <i>version 9.1 (R2016b)</i>	Natick, Massachusetts: The MathWorks Inc.	<a href="https://www.mathworks.com/">https://www.mathworks.com/</a>
Grassberger-Procaccia algorithm	<a href="#">Grassberger and Procaccia, 1983</a>	N/A
Trichome model simulations in MATLAB	This study	<a href="https://github.com/AnnaDeneer/Trichome-Model">https://github.com/AnnaDeneer/Trichome-Model</a>

**RESOURCE AVAILABILITY**

**Lead contact**

Further information and/or requests for resources, reagents, and data should be directed to and will be fulfilled by the Lead Contact, Dr. Martin Hülskamp ([martin.huelskamp@uni-koeln.de](mailto:martin.huelskamp@uni-koeln.de)).

**Materials availability**

All unique/stable reagents generated in this study are available from the Lead Contact with a completed Materials Transfer Agreement.

**Data and code availability**

The modeling software developed in this study can be downloaded from: <https://github.com/AnnaDeneer/Trichome-Model>

## EXPERIMENTAL MODEL AND SUBJECT DETAILS

*Arabidopsis thaliana* was grown under standard long day (16 h light and 8 h dark) conditions at 22°C temperature. Transgenic plants were generated following the floral dip method (Clough and Bent, 1998). The reporter lines *pTRY:GUS* and *pCPC:GUS* (Pesch and Hülkamp, 2011) were introduced in *ttg1* mutants by backcrosses and selection of plants homozygous for *ttg1* and the GUS reporter construct.

## METHOD DETAILS

### Analysis of fluorescence intensity in trichomes and surrounding tiers

Stable lines expressing TTG1 tagged with YFP and the three TTG1 mutant proteins tagged with YFP under the control of the TTG1 promoter were analyzed using confocal laser scanning microscopy. The DM6000 CS Microscope was used in combination with the TCS-SP8 imaging system (Leica Microsystems, Heidelberg, Germany). Z stacks of young trichomes and surrounding tiers were acquired with a plane thickness of around 1–1.5 μm using the 20x water immersion objective. Determination of fluorescence intensity was achieved by using the software ImageJ (Fabrice Cordeliers, Institute Curie, Orsay, France). Maximum projections of the planes displaying the trichome and the surrounding tiers of cells were created, and fluorescence intensity (mean gray value) was measured in manually placed ROIs (region of interest). For each trichome three elliptical ROIs were chosen (Figure S3A). In the epidermal cells three polygonal ROIs were selected in each tier in the cytoplasmic regions (Figure S3A). The mean fluorescence for the trichome and each of the three tiers were calculated. Trichome fluorescence intensity was set to 100% and for each tier the fluorescence percentage compared to the trichome intensity was calculated. Subsequently for each YFP-tagged TTG1 allele the mean percentage of the 1<sup>st</sup>, 2<sup>nd</sup> and 3<sup>rd</sup> tier was calculated as well as the standard deviations (TTG1 n = 12, TTG1-9 n = 19, TTG1-11 n = 28, TTG1-12 n = 15). The data were tested for normal distribution using the Kolmogorov-Smirnov test ( $\alpha = 0.05$ ) followed by a one-sample t test ( $p = 0.002$ ). All calculations were performed using Microsoft Excel 365.

### Light microscopy

To observe the root phenotypes of wild-type (Col-0), *ttg1-1*, *ttg1-9*, *ttg1-11* and *ttg1-12*, seeds were sterilized and sown on ½ MS plates with 1% sugar. After 2 days of stratification the plates were transferred into a growth chamber (22°C, light/dark cycle of 16/8 h, humidity of 60%) and placed vertically. 2–3 days later the seedlings were transferred to a microscopic slide wrapped with parafilm on both ends so that the seedlings all had the cotyledons on one long side of the slide. Liquid 1/10 MS with 1% sugar was added to the roots and the plants, except for the leaves, were covered with a cover slide. The slides were placed vertically into a glass box filled with some 1/10 MS with 1% sugar and stored in the growth chamber. After one day the roots were examined using the DM5000 B and the DFC360 FX imaging system (Leica Microsystems, Heidelberg, Germany).

Seed color was examined using a LEICA MZ16 F and documentation was performed by using the LEICA DFC420 C imaging system.

To analyze seed coat mucilage production by seed epidermal cells, a ruthenium red staining was performed. Seeds were hydrated in water for 5 min under gentle shaking. After removing the water, ruthenium red solution (0.1 mg/ml) was added. After 5 min of incubation the seeds were washed twice with water (Western et al., 2000) and examined using a LEICA MZ16 F and documentation was performed by using the LEICA DFC420 C imaging system.

Trichome coordinates of Col-0 and *ttg1-9* were extracted using TrichEratops (Failmezger et al., 2013).

GUS analysis was performed as described previously (Sessions et al., 1999). Light microscopy was done either using a Leica MZ16F binocular microscope or a Leica DMRE microscope equipped with a high resolution KY-F70 3-CCD JVC camera and DISKUS software. Confocal laser scanning microscopy was performed on Leica TCS-SP2 imaging system (Leica Microsystems) equipped with LCS software. 40x water immersion objective was used to obtain the z stack images. z stack images were merged to obtain the image in one plane. YFP fluorescence quantification was done using the histogram quantification tool in LCS software.

### Yeast two hybrid and nuclear transport assays

For protein-protein interaction in yeast, pAS2 and pC-ACT2 plasmids (Clontech) were used for translational fusion of proteins either with GAL4 activation or DNA binding domain respectively. *TTG1*, *TTG1-13*, *TTG1-9*, *TTG1-11* and *TTG1-12* were cloned as a fusion to DNA binding domain in the pAS2 vector and *GL3*, *EGL3* and *TT8* were cloned as a fusion to the GAL4 activation domain by LR clonase reaction. *Saccharomyces cerevisiae* strain AH109 was transformed as described previously for the interaction assay (Gietz et al., 1995).

Yeast Nuclear Transportation Trap (NTT) assay was performed in yeast strain EGY48 as described before (Ueki et al., 1998). NTT constructs pNH2 (NES-LexAD), pNS (modified pNH2) (Ueki et al., 1998), pNS-TTG1, pNS-TTG1-13 and pVT-U-GL3 (Balkunde et al., 2011) have been described before. pNS-TTG1-9, pNS-TTG1-11 and pNS-TTG1-12 were created by cloning Sall and XhoI fragments from corresponding entry vectors into the Sall site in pNS vector to obtain pNS-TTG1-9, pNS-TTG1-11 and pNS-TTG1-12. Yeast harboring pNS and pVT-U plasmids grow on synthetic dropout media lacking histidine and uracil respectively. Transport of protein of interest as a translational fusion to NES-LexAD into the nucleus results in activation of *rhw* leucine reporter gene under GAL4 promoter and is read out by growth of yeast cells on the synthetic dropout media lacking amino acid leucine.

## LUMIER

Two destination vectors were used for LR reactions. pcDNA3-Rluc-GW and pTREXdest30 (Invitrogen) enable the N-terminal fusion of *Renilla reniformis* and *Staphylococcus aureus* proteins, respectively (Pesch et al., 2013). GL3 was N-terminally fused to the *S. aureus* ProtA sequence in pTREX-dest30-ntPrA. As a negative control, the vector pTREX-dest30-ntPrA was recombined with pENTR1A-w/o-ccdB. *R. reniformis* Luciferase-TTG1-wt, Luciferase-TTG1-9, Luciferase-TTG1-11 and Luciferase-TTG1-12 were created as N-terminal fusions in pcDNA3-Rluc-GW. pENTR1A-w/o-ccdB was used as a negative control. For LUMIER assays, each protein was transiently expressed in HEK293TN cells (BioCat/SBI; LV900A-1). Transfection and pull down assay were done as described before (Pesch et al., 2013, 2015) three times independently each as two technical replicas

## Constructs

All entry clones were in pENTRY1A/pENTR4. TTG1-YFPpEN (Bouyer et al., 2008), TTG1ΔC26-YFPpEN where carboxy terminal 26 amino acids are deleted (Balkunde et al., 2011) and TTG1pEN (Pesch et al., 2015) have been described previously. TTG1-9-YFPpEN, TTG1-11-YFPpEN for *ttg-11* and TTG1-12-YFPpEN were generated by site directed mutagenesis using TTG1-YFPpEN as a template. Entry clones of all the *ttg1* allelic versions without YFP fusion were also generated by site directed mutagenesis using TTG1pEN as a template. For plant transformation all the TTG1-YFP versions were cloned into pAMPAT-pTTG1-GW binary vector (Bouyer et al., 2008) by LR clone reaction to express them under native TTG1 promoter.

## Generation of a random pattern

We compare the data from leaves to a suitable random reference. There are two requirements the random patterns should fulfil. First, the points should be independent and identically distributed, i.e., we assume complete spatial randomness. Second, the amount and variation in density of points per representation should reflect the observations for wild-type and *ttg1-9* phenotypes. For these reasons we simulate a homogeneous Poisson point process (Holgate, 1965). We generate  $10^4$  random representations for both wild-type and *ttg1-9*. For each of these representations the points density is sampled from a Poisson distribution using the mean trichome density determined from either the wild-type or *ttg1-9* leaves as a parameter for the distribution. The points for each representation are uniformly and independently placed within the unit circle.

## Quantification of the regularity of patterns

To quantify the regularity of the trichome patterns we focus on two measures. The first measure is the coefficient of variation of nearest neighbor distances. For each leaf (wild-type and *ttg1-9*) we calculate the Euclidian distances for each trichome  $\delta_i$  for each trichome  $t_i$  to its nearest neighbor  $t_n$  by

$$\delta_i = \sqrt{(x_i - x_n)^2 + (y_i - y_n)^2} \quad (1)$$

where  $(x_i, y_i)$  are the coordinates for trichome  $t_i$  and  $(x_n, y_n)$  the coordinates for its nearest neighbor  $t_n$ . Next, we use the coefficient of variation (ratio of the standard deviation of the distances  $\delta^\sigma$  to the mean  $\bar{\delta}$ ) of the nearest neighbor distances which is defined by

$$CV_{NN} = \frac{\delta^\sigma}{\bar{\delta}} \text{ with } \bar{\delta} = \frac{1}{|\mathcal{T}_k|} \sum_{i=1}^{|\mathcal{T}_k|} \delta_i \text{ and } \delta^\sigma = \sqrt{\frac{1}{|\mathcal{T}_k| - 1} \sum_{i=1}^{|\mathcal{T}_k|} (\delta_i - \bar{\delta})^2} \quad (2)$$

where  $\mathcal{T}_k$  is the set of trichome coordinates for a certain leaf  $k$  and  $|\mathcal{T}_k|$  its cardinality. The  $CV_{NN}$  reported for wild-type and *ttg1-9* is the mean of  $n = 9$  and  $n = 11$  leaves respectively.

In addition to the  $CV_{NN}$  we use the mean anisotropy as a measure of pattern regularity. The anisotropy has been shown to be a suitable measure of the local trichome environment (Greese et al., 2012). Following the procedure from Greese et al., we determine the ratio of eigenvalues of the inertia tensor for each trichome. We report the average of these ratios for each leaf and averaging again over all leaves (or computer-generated patterns).

## Theoretical probability of finding clusters in random patterns

For a homogeneous Poisson process the probability to find  $n$  points per unit area is given by the Poisson distribution:

$$P(n) = \frac{m^n e^{-m}}{n!} \quad (3)$$

where  $m$  is the mean number of points per area. Because we consider a homogeneous process the probability is independent of the specific location of area of interest. If  $\rho$  is the mean density of the distribution, then  $m = \pi r^2 \rho$ , which upon substitution into Equation 3 gives:

$$P(n) = \frac{\pi r^2 \rho^n e^{-\pi r^2 \rho}}{n!} \quad (4)$$

The probability of the chosen area  $\pi r^2$  containing no points is

$$P_0(r) = P(n = 0) = e^{-\pi r^2 \rho} \quad (5)$$

which is the probability that the area within a distance  $r \geq 0$  contains no points. Consequently, the probability of finding at least one point within a radius  $r$  is given by:

$$P_{\geq 1}(r) = 1 - e^{-\pi r^2 \rho}. \quad (6)$$

The relation given in Equation 6 is visualized in Figure S2A for densities corresponding to wild-type and *ttg1-9*. For a random pattern of lower density, the probability of finding a cluster is lower than for a pattern of higher density.

### Correlation dimension of experimental data and simulated patterns

The correlation dimension can be used to evaluate the number of factors that are involved in the variability of a process (Sandler et al., 2015; Skinner, 1994). In this case we are interested in the application of the correlation dimension in spatial patterns. For the trichome and randomly generated patterns we use the Grassberger-Procaccia algorithm to extract the correlation dimension from the data (Grassberger and Procaccia, 1983). The spatial coordinates are given in two dimensions; therefore, the maximum correlation dimension is two. This maximum dimension is found back in the analysis of the random data, showing that there is no underlying deterministic factor in determining the pattern (Figures S2C–S2F). For both the wild-type and the *ttg1-9* data we find correlation dimensions  $< 2$ , indicating that there is some inherent deterministic mechanism operating in the patterning of both phenotypes.

### Reproducing trichome pattern irregularity by perturbing hexagonal patterns

To reflect the noise level of nearest neighbor distances of trichomes seen in wild-type ( $CV_{NN} = 0.33$ ), we apply a random perturbation to the coordinates of a completely regular hexagonal pattern consisting of  $n = 100$  points. Considering that wild-type phenotypes do not show any clusters of trichomes, we include an exclusion zone around every point. This exclusion zone is achieved by defining a region around a certain point with a radius  $z$ . The algorithm for generating the perturbed pattern is the following:

1. Generate  $u_1, u_2, \dots, u_N \sim \mathcal{U}(0, 1)$  independently.
2. Set  $R_1 \leftarrow r\sqrt{u_1}, R_2 \leftarrow r\sqrt{u_2}, \dots, R_N \leftarrow r\sqrt{u_N}$ .
3. Generate  $u_{N+1}, u_{N+2}, \dots, u_{2N} \sim \mathcal{U}(0, 1)$  independently.
4. Set  $\Theta_1 \leftarrow 2\pi u_{N+1}, \Theta_2 \leftarrow 2\pi u_{N+2}, \dots, \Theta_N \leftarrow 2\pi u_{2N}$ .
5. Select points  $(x_i, y_i)$  by a random permutation on the integers  $I = \{1, \dots, N\}$ .
6. Set  $x_1 \leftarrow x_1 + R_1 \cos\Theta_1, x_2 \leftarrow x_2 + R_2 \cos\Theta_2, \dots, x_N \leftarrow x_N + R_N \cos\Theta_N$
7. Set  $y_1 \leftarrow y_1 + R_1 \sin\Theta_1, y_2 \leftarrow y_2 + R_2 \sin\Theta_2, \dots, y_N \leftarrow y_N + R_N \sin\Theta_N$
8. For steps 6 and 7 check if the nearest neighbor distance from point  $i \in I$  is larger than  $z = 0.4$ , else point  $(x_i, y_i)$  is not shifted.

This exclusion zone in step 8 of  $z = 0.4$  is arbitrarily chosen, but sufficient to reproduce a  $CV_{NN}$  corresponding to measurements of wild-type leaves.

Next, we generated a vector of points by drawing from  ${}^n P_r$ , with  $n = 100$  and  $r = 54$ . The coordinates corresponding to the integers in this vector are removed from the grid, yielding a density relative to the wild-type grid of 0.46.

Finally, we induce clustering by first selecting 8 points out of the 46 remaining after sparsening by random permutation. Next, the selected points are split into two groups of 4 points. The coordinates of the second group are set to the coordinates of the first group plus a value smaller than the minimal nearest neighbor distance found in the previous step. This set of points is then counted as clusters, giving a density of 8 out of 46 (18%), comparable to experimental observations. The pattern showing clusters and a reduced density has a  $CV_{NN}$  similar to the *ttg1-9* leaves ( $CV_{NN} = 0.85$ ). Edges between points are determined by MATLAB's built-in Delaunay Triangulation function.

### Trichome patterning model

The cells are modeled on a hexagonal grid of  $N_x$  by  $N_y$  cells with periodic boundary conditions based on a modeling framework described before (Bouyer et al., 2008; Digiuni et al., 2008). Transport of species  $\chi$  between cell  $j$  at coordinates  $(x, y)$ , where  $1 \leq x \leq N_x$  and  $1 \leq y \leq N_y$  and its neighbor is modeled by the coupling equation

$$\widehat{L}[\chi]_{x,y} = [\chi]_{x,y-1} + [\chi]_{x,y+1} + [\chi]_{x-1,y} + [\chi]_{x+1,y} + [\chi]_{x+1,y-1} + [\chi]_{x-1,y+1} - 6[\chi]_{x,y}. \quad (7)$$

Based on the network presented in Figure 7E, we used the following system of dimensionless coupled ordinary differential equations (ODEs) to describe the change over time of TTG1, GL1, GL3, TRY, CPC and the active complex between TTG1-GL3 (AC1) and GL1-GL3 (AC2):

$$\partial_t [TTG1]_j = k_1 - [TTG1]_j (k_2 + k_3 [GL3]_j) + k_2 k_3 \widehat{L}[TTG1]_j \quad (8)$$

$$\partial_t[GL1]_j = k_5 + k_6[AC2]_j - [GL1]_j(k_7 + k_8[GL3]_j) \quad (9)$$

$$\partial_t[GL3]_j = k_9 + \frac{k_{24}k_{10}[AC1]_j^2}{k_{24} + [AC1]_j^2} + \frac{k_{23}k_{11}[AC2]_j^2}{k_{23} + [AC2]_j^2} - [GL3]_j(k_{12} + k_3[TTG1]_j + k_8[GL1]_j + k_{13}[TRY]_j + k_{14}[CPC]_j) \quad (10)$$

$$\partial_t[TRY]_j = k_{15}[AC1]_j^2 + k_{25}[AC2]_j^2 - [TRY]_j(k_{16} + k_{13}[GL3]_j) + k_{16}k_{17}\widehat{L}[TRY]_j \quad (11)$$

$$\partial_t[CPC]_j = k_{18}[AC2]_j^2 - [CPC]_j(k_{19} + k_{14}[GL3]_j) + k_{19}k_{20}\widehat{L}[CPC]_j \quad (12)$$

$$\partial_t[AC1]_j = k_3[GL3]_j[TTG1]_j - k_{21}[AC1]_j \quad (13)$$

$$\partial_t[AC2]_j = k_8[GL3]_j[GL1]_j - k_{22}[AC2]_j \quad (14)$$

The first version of the model consisted only of Equations 8, 10, 11, and 13 and a smaller amount of parameters, giving the network of black edges only in Figure 7E. This was extended later by including Equation 9 and Equation 14, this is the combination of black and light green edges in Figure 7E. Finally, CPC was included through Equation 12, resulting in the complete network. Note that parameter  $k_{25}$  is generally set to 0 except in the pCPC:TRY rescue simulation where  $k_{25} > 0$  (Figure S7D).

### Pattern quantification

Similar to the hexagonal point pattern analysis, we determined the coefficient of variation of the nearest neighbor distances ( $CV_{NN}$ ), cluster density and trichome density for the model simulations. In order to calculate any of the quantities we first identified the trichome cells. Toward that end, the steady-state concentrations of the active complex  $[AC]_{x,y}$  are normalized by the maximum observation  $[AC]_{max}$ ; cells that contain more than half-maximum of AC are classified as trichomes. In the model with both the GL3-TTG1 (AC1) and GL3-GL1 (AC2) active complex the sum of both complexes is used, i.e.,  $[AC]_{x,y} = [AC1]_{x,y} + [AC2]_{x,y}$ . Using these criteria we can identify the set of grid-coordinates at which trichomes can be found, formally defined as  $\mathcal{T} = \{(x, y) | [AC]_{x,y} \geq (1/2)[AC]_{max}\}$ . The number of elements in this set, i.e., its cardinality  $|\mathcal{T}|$ , equals the number of trichomes on the grid. By dividing the cardinality by the total number of cells (grid size) we obtain the trichome density. Next, we determined the cluster frequency by identifying the elements with coordinates that are next to each other on the grid and by dividing that number by  $|\mathcal{T}|$ . Finally, we determined the nearest neighbor distances. For this we considered the trichome cells as a point pattern on a hexagonal grid. With the set of coordinates of trichomes on this grid we used MATLABs *knnsearch* with default settings. From this distribution of distances we determine the  $CV_{NN}$ , as described above.

### Parameter scan

As all parameters for the system are unknown, we used Latin Hypercube sampling to study system dynamics at different points in the parameter space. Within the parameter space there exists a sub-space where Turing patterning can occur, called the Turing Space. In this domain a diffusion-driven instability (Turing instability) can occur resulting in an inhomogeneous patterning state (Turing, 1952). To test this for our randomly generated sets we use linear stability analysis where the stability of a uniform steady state is verified by determining whether effects of small perturbations to the ODE system decay over time. Turing instability was tested by the following criteria: starting from a uniform steady state (i) the steady state in the absence of diffusion is stable and (ii) the steady state in the presence of diffusion is unstable (Murray, 2002). For criterion i this means that all eigenvalues of the Jacobian evaluated at steady state must be negative. To perform the same test for criterion ii we decoupled the system by Fourier transformation and analyzed the eigenvalues (Bouyer et al., 2008; Digiuni et al., 2008), where the real part of at least one of the eigenvalues must be positive.

### Parameter criteria

To test in the mathematical model whether the patterning defects can be explained by a reduced binding of TTG1 to GL3 ( $\beta$ ) this parameter is varied while other factors are kept constant.

In a random parameter search, the parameter sets are tested for (i) Turing instability, (ii) increase in cluster densities, (iii) relative increase in CV (iv) a relative decrease in trichome densities. Every quantity is fitted to the following experimentally determined ranges: trichome density of  $0.46 \pm 0.06$  relative to wild-type, CV of  $2.22 \pm 0.22$  relative to wild-type and a cluster density of  $0.18 \pm 0.07$ .

After an initial search of  $10^6$  randomly generated parameter sets we found 4 sets that fitted these criteria. These sets were then used to define a local search area to speed up the parameter search. With this approach we found 40 parameter sets that were used to study the pattern development for decreasing TTG1-GL3 interaction strengths.

For parameter sets that match the criteria, the quantitative factors, e.g., cluster density, were averaged across multiple simulations with randomly perturbed initial conditions until convergence. Convergence is defined as  $(\sigma / \sqrt{N}) < \varepsilon \cdot \theta(k)$  where  $\sigma$  is the standard deviation of a pattern quantity,  $N$  the number of simulation repeats,  $\varepsilon$  a measure of accuracy, which we set to 0.05, and  $\theta(k)$  the mean of a pattern quantification (e.g., trichome density) for parameter set  $k$ .

### Depletion in the activator-depletion model

For the simplest combination of the AI and AD model networks, we found that loss of depletion in the *ttg1-9* mutant simulations was not observed, in fact we found a focusing effect where more TTG1 was recruited to trichome cells. To facilitate the analysis we focused on the behavior of the AD sub-motif. As expected, reduced binding strength resulted in higher amount of free TTG1 (Figure S5B), which in turn results in a higher effective TTG1 mobility (Figure S5A). The number of peaks (i.e., trichomes) was decreased and the peak height (i.e., AC levels in trichomes) was increased (Figure S5B). As a consequence, also TTG1 was more strongly focused in the trichomes.

We further sought to gain insight into the underlying reason of the focusing effect. A reduction of the interaction rate between TTG1 and GL3 results in an enhanced number of unstable Fourier modes (Figure S5C) for the initial Turing instability (see section on ‘Dispersion relation’ below for methods). Due to this, only the major peaks of the stochastic initial perturbation grow into stable large peaks. Because TTG1 is less bound in complexes in non-peak cells, more TTG1 can be recruited to the developing peaks. This results in low trichome density with enhanced peak height and strong depletion of TTG1 around peak cells. This is contrasted by the wild-type situation where only very few Fourier modes are unstable (Figure S5B). From the stochastic initial perturbation only the high-frequency modes are selected while most Fourier modes are damped. This means that the AD motif acts as a spatial high-pass filter.

### Dispersion relation

When the binding strength between TTG1 and GL3 is decreased less AC is formed. This observation is confirmed by the model and is one of the possible reasons why the trichome density is decreased for the mutants. To determine the effect of the change in binding strength on the pattern formation, the dispersion relation is studied for different binding strengths on a 1-dimensional grid of  $N$  cells. The Fourier modes for a 1D grid are given by

$$k^2 = 4 \sin^2 \left( \frac{\pi n}{N} \right) \quad (15)$$

where  $1 \leq n \leq N$ , and

$$\mathbf{A}_{p,q} = \mathbf{J}_0 - \mathbf{D}k^2 \quad (16)$$

where  $\mathbf{J}_0$  is the Jacobian evaluated at steady state and  $\mathbf{D}$  is the diffusion matrix. The eigenvalues for the matrix  $\mathbf{A}_{p,q}$  are determined for different wavenumbers and different values for the binding strength parameter. Given that a pattern is only formed when  $Re(\lambda) > 0$  the dispersion relation shows which wavenumbers correspond to unstable modes and are thus a possible component of the pattern.

### QUANTIFICATION AND STATISTICAL ANALYSIS

For the statistical analysis of the difference of the mean intensity in trichomes and the three neighboring epidermal cell tiers the data were first tested for normal distribution using the Kolmogorov-Smirnov test ( $\alpha = 0.05$ ) followed by a one sample t test ( $p = 0.002$ ). All calculations were performed using Microsoft Excel 365.

For testing the statistical difference in pattern irregularity for the mean  $CV_{NN}$  and anisotropy Mann-Whitney U-test was used ( $\alpha = 0.01$ ). The single-tailed test was used to test whether the irregularity measures were greater for random patterns than wild-type and whether *ttg1-9* patterns were more irregular than wild-type. In comparing *ttg1-9* to random patterns we tested whether *ttg1-9* was more irregular than the random reference patterns.